Intra-mitochondrial proteostasis

is directly coupled to alpha-synuclein and Amyloid β 1-42 pathology

Janin Lautenschläger[1*], Sara Wagner-Valladolid[1], Amberley D. Stephens[1], Ana Fernández-Villegas[1], Colin Hockings[1], Ajay Mishra[1], James D. Manton[2], Marcus J. Fantham[3], Meng Lu[1], Eric J. Rees[2], Clemens F. Kaminski[3], Gabriele S. Kaminski Schierle[1*]

[1] Molecular Neuroscience Group, Department of Chemical Engineering and Biotechnology, University of Cambridge, West Cambridge Site, Philippa Fawcett Drive, Cambridge, CB3 0AS, UK; [2] Quantitative Imaging Group, Department of Chemical Engineering and Biotechnology, University of Cambridge, West Cambridge Site, Philippa Fawcett Drive, Cambridge, CB3 0AS, UK; [3] Laser Analytics Group, Department of Chemical Engineering and Biotechnology, University of Cambridge, West Cambridge Site, Philippa Fawcett Drive, Cambridge, CB3 0AS, UK

* Corresponding authors:

Janin Lautenschläger, Gabriele S. Kaminski Schierle

Email: janin.lautenschlaeger@gmail.com, gsk20@cam.ac.uk

Molecular Neuroscience Group, Department of Chemical Engineering and Biotechnology

University of Cambridge, West Cambridge Site, Philippa Fawcett Drive, Cambridge, CB3 0AS, UK

26   **Abstract**

27   Mitochondria have long been implicated in Parkinson's disease (PD), however, it is not clear

28   how mitochondrial impairment and alpha-synuclein pathology are coupled. We report here

29   that intra-mitochondrial protein homeostasis plays a major role in alpha-synuclein fibril

30   elongation, as interference with intra-mitochondrial proteases and mitochondrial protein

31   import significantly aggravate alpha-synuclein aggregation. In contrast, direct inhibition of

32   mitochondrial complex I, increase in intracellular calcium concentration or formation of

33   reactive oxygen species (ROS), all of which have been associated with mitochondrial stress,

34   did not affect alpha-synuclein pathology. We further demonstrate that similar mechanisms

35   are involved in Amyloid β 1-42 (Aβ42) aggregation, suggesting that mitochondria are directly

36   capable of influencing cytosolic protein homeostasis of aggregation-prone proteins.

37

38

39

40

41

42

43

44

45

47

48

49

50   **Introduction**

51

52   Parkinson's disease (PD) is the second most common neurodegenerative disease and affects

53   about 1% of the population over 60 years (1). Alpha-synuclein aggregation has been found

54   central to the disease, since SNCA mutations are associated with familiar PD (2) and alpha-

55   synuclein has been identified as a major constituent of Lewy bodies in sporadic PD and

56   dementia with Lewy bodies (3). A relationship between protein aggregation and protein levels

57   is demonstrated by familiar PD with SNCA gene duplication and triplication (4–6), however

58   the trigger for protein aggregation in sporadic cases is less clear. Likewise, also Alzheimer's

59   disease is linked to increased protein aggregation, where enhanced levels of Amyloid beta

60   (Aβ) due to mutations in the genes coding for the amyloid precursor protein (APP) (7, 8) or

61   presenilin (9–11) are found in familiar AD.

62

63   Mitochondria have long been implicated in PD, ever since the discovery that inhibitors of the

64   mitochondrial complex I can lead to dopaminergic neuron death (12–16). But also the

65   regulation of mitophagy via the PTEN-induced kinase 1 (PINK1) plays a role in PD (17) and

66   seems to be coupled to alpha-synuclein toxicity. PINK1 overexpression is able to decrease the

67   effect of alpha-synuclein toxicity in Drosophila (18, 19), and PINK1 knockout in mice increases

68   alpha-synuclein neurotoxicity (20, 21). Furthermore, PINK1 patient iPSC-derived midbrain

69   dopaminergic neurons show accumulation and aggregation of alpha-synuclein (Chung *et al*,

70   2016), and PINK1 knockout rats even show alpha-synuclein de novo aggregation (24).

71

72   We have demonstrated previously that alpha-synuclein interaction with calcium leads to

73   conformational changes at the C-terminus of alpha-synuclein, but also at the aggregation-

3

74   prone non-amyloid component (NAC)-region, suggesting that calcium can directly influence

75   the aggregation propensity of alpha-synuclein (25). Thus, we tested, whether treatment with

76   BAPTA-AM, which is supposed to decrease intracellular calcium by calcium chelation, was able

77   to decrease alpha-synuclein pathology. However, we observed drastically enhanced alpha-

78   synuclein aggregation, which we could attribute to mitochondrial fragmentation. This led us

79   to study and show that disturbances in intra-mitochondrial proteostasis can aggravate alpha-

80   synuclein aggregation. We identified that the Lon protease and the high-temperature

81   requirement protein A2 (HtrA2) protease, as well as mitochondrial protein import are crucial

82   in determining the level of alpha-synuclein seeding in a cellular model. However, inhibition of

83   the mitochondrial complex I and a direct increase in cytosolic calcium or oxidative stress were

84   not able to reproduce enhanced alpha-synuclein pathology such as observed in cells upon

85   inhibition of mitochondrial protein homeostasis. In addition, the mitochondrial protease

86   HtrA2 and mitochondrial protein import were also relevant for Aβ42 aggregation and isolated

87   mitochondria were shown to directly diminish Aβ42 aggregation.

88

89

90   **Results**

91

92   **BAPTA-AM increases alpha-synuclein pathology**

93

94   SH-SY5Y cells overexpressing YFP-alpha-synuclein were incubated for 4 hours (h) with small

95   fibrillar seeds made of unlabelled human recombinant alpha-synuclein to study alpha-

96   synuclein pathology after seeding, as described previously (26–30). Cells were left in culture

97   for 3 days before the level of alpha-synuclein aggregation within the cells was determined (see

4

98   Supplementary Fig. 1A and B for treatment regime and fibrillar seeds). While unseeded YFP-

99   alpha-synuclein overexpressing cells did not display any aggregates, those that were seeded

100   displayed large YFP-alpha-synuclein aggregates which were built up from fine filaments

101   (Supplementary Fig. 1C). Furthermore, YFP-alpha-synuclein inclusions stained positive for

102   ubiquitin and p62, which are both characteristic markers of Lewy bodies in human disease

103   (26) (Supplementary Fig. 1D and E).

104

105   We have previously shown that alpha-synuclein strongly interacts with calcium, leading to

106   conformational changes both at the C-terminal calcium-binding domain, and the aggregation-

107   prone non-amyloid component (NAC)-region, which suggests that calcium can directly

108   influence the aggregation propensity of alpha-synuclein. Consistently, increased calcium

109   concentrations significantly enhanced alpha-synuclein nucleation in vitro (25). BAPTA-AM as

110   a calcium chelator is supposed to decrease cytosolic calcium and has been previously reported

111   to alleviate KCl-induced alpha-synuclein aggregation (31). However, when we treated the

112   above-described cells with BAPTA-AM before the incubation with fibrillary seeds (1h) or

113   before and during incubation with fibrillary seeds (5h) alpha-synuclein seeding was drastically

114   increased (Fig. 1A). We thus tested the calcium effect of BAPTA-AM in SH-SY5Y cells and

115   verified that BAPTA-AM was able to decrease cytosolic calcium. However, the effect was only

116   transient and calcium chelation was already compensated in cells treated for 1 h and 5 h (Fig.

117   1B, fluorescence lifetime decrease after 10 min from 2381+/-8 ps to 2170+/-15 ps, lifetime of

118   2400 +/-8 ps after 1h and 2460+/-12 ps after 5h). Since the 1 h treatment showed calcium

119   levels comparable to control, but already increased alpha-synuclein aggregation, suggested

120   that the increase of alpha-synuclein seeding by BAPTA-AM was not mediated via calcium. In

121   addition, we tested whether both the ester form of BAPTA, BAPTA-AM, as well as the active

5

122　BAPTA itself affected the aggregation of alpha-synuclein directly, but found no difference in

123　alpha-synuclein aggregation kinetics measured in-vitro by Thioflavin T (ThT) fluorescence (Fig.

124　1C, t_{50} 125.6+/-8.6 h and 122.6+/-7.2 h vs. 116.6+/-11.1 h). This confirms that the effect of

125　BAPTA is most likely triggered by a cellular response. In the literature there was one report

126　describing that BAPTA-AM can lead to mitochondrial fragmentation (32), so we stained our

127　cells with Mitochondria-RFP and indeed observed a drastic mitochondrial fragmentation upon

128　BAPTA-AM treatment (Fig. 1D).

129

130　Thus, it seems that mitochondrial dysfunction influences alpha-synuclein aggregation per se,

131　which we tested using carbonyl cyanide 4-(trifluoromethoxy)phenylhydrazone (FCCP), a

132　mitochondrial uncoupler which dissipates the mitochondrial membrane potential. Treatment

133　with FCCP during alpha-synuclein fibril incubation (5h) increased alpha-synuclein seeding (Fig.

134　1E), however FCCP did not increase alpha-synuclein aggregation in-vitro (t_{50} 117.0+/-9.8 h vs.

135　115.6+/-10.1 h), confirming that its effect in cells is the result of a cellular response rather

136　than a direct interaction of FCCP and alpha-synuclein (Fig.1F).

137

138

139　**Classical downstream effectors of mitochondrial dysfunction are unable to influence alpha-**

140　**synuclein pathology**

141

142　We next tested whether downstream events of mitochondrial dysfunction could reproduce

143　increased alpha-synuclein seeding. However, if we inhibited mitochondrial ATP production via

144　inhibition of complex I, directly increased cytosolic calcium or oxidative stress for 3 days until

145　seeding was evaluated, no increase in alpha-synuclein seeding was seen (Fig. 2A). We used 1-

146   methyl-4-phenylpyridinium (MPP$^+$), the active metabolite of 1-methyl-4-phenyl-1,2,3,6-

147   tetrahydropyridine (MPTP) to inhibit complex I of the electron transport chain, ionomycin, an

148   ionophore, to increase cytosolic calcium concentrations via calcium influx through the plasma

149   membrane, and menadione to induce the formation of ROS via redox-cycling (33). To test that

150   the inhibitors were active we measured ATP, calcium and H_2O_2 in SH-SY5Y cells using the

151   fluorescent sensors Ateam1.03, Oregon-Green^{TM} BAPTA-1 and HyPer. The readout of the

152   fluorescence lifetime of these sensors allows to estimate and directly compare the different

153   treatments (34, 35). So, MPP$^+$ inhibition of complex I reduced the ATP level (Fig. 2B,

154   fluorescence lifetime increase of the FRET donor from 1298 +/- 17 ps to 1511 +/- 20 ps),

155   ionomycin increased cytosolic calcium (Fig. 2C, fluorescence lifetime increase of Oregon-

156   Green^{TM} BAPTA-1 from 2381 +/- 8 ps to 2663 +/- 7 ps), and menadione increased H_2O_2 levels

157   (Fig. 2D, fluorescence lifetime decrease of cpYFP from 1575 +/- 4 ps to 1557 +/- 3 ps).

158   Treatment with MPP$^+$ lead to lower ATP depletion than under FCCP, but to higher ATP

159   depletion than under BAPTA-AM (Fig. 2B). Ionomycin treatment lead to higher calcium

160   increase compared to both, FCCP and BAPTA-AM (Fig 2C). And menadione treatment lead to

161   comparable levels of H_2O_2 increase than under treatment with FCCP and BAPTA-AM (Fig. 2D).

162   This suggests that complex I inhibition, cytosolic calcium increase and oxidative stress do not

163   aggravate alpha-synuclein pathology per se.

164

165

166   **Inhibition of mitochondrial proteostasis increases alpha-synuclein pathology**

167

168   In the next step we evaluated mitochondrial fragmentation upon treatment with FCCP and

169   BAPTA-AM, as well as MPP$^+$, ionomycin and menadione. Automated analysis of mitochondrial

7

170   length showed that both FCCP and BAPTA-AM treatment leads to mitochondrial

171   fragmentation, while neither MPP⁺, nor ionomycin or menadione influenced mitochondrial

172   integrity (Fig. 3A and B). Furthermore, we saw that FCCP treatment led to higher levels of

173   mitochondrial fragmentation compared to BAPTA-AM, though the effect of BAPTA-AM on

174   alpha-synuclein seeding was more pronounced than after FCCP treatment (refer to Fig. 1A and

175   E). This indicated that mitochondrial fragmentation is not directly linked to alpha-synuclein

176   aggregation and additional factors might play a role.

177

178   Previously, BAPTA-AM has been reported to inhibit proteases (36–38), which is mediated via

179   the blocking of intracellular calcium transients required to regulate protease activity (39, 40).

180   This led us to test the effect of mitochondrial proteostasis on alpha-synuclein pathology. We

181   treated the YFP-alpha-synuclein SH-SY5Y cells with CDDO-Me, an inhibitor of the Lon protease

182   (41), which has recently been shown to influenced aggregate dissolution after heat shock (42)

183   and also with UCF-101, an inhibitor of the high temperature requirement protein A2

184   (HtrA2/Omi) protease (43), which has previously been linked to PD. Our results show that both

185   mitochondrial protease inhibitors significantly increased alpha-synuclein pathology (Fig. 3C),

186   where the effect of HtrA2 protease inhibition was superior to Lon protease inhibition.

187

188

189   **Inhibition of mitochondrial proteostasis increases Amyloid β 1-42 pathology**

190

191   To test if the above-discussed mechanisms also contribute to the aggregation of other

192   proteins involved in neurodegeneration, we investigated the effect of mitochondrial

193   proteostasis on Amyloid β 1-42 (Aβ42) pathology. We used a stable HEK cell line

8

194 overexpressing Aβ42-mCherry via a tetracycline-inducible expression system as published

195 previously (44). After induction of Aβ42-mCherry expression, the cells were treated with FCCP,

196 BAPTA-AM and the protease inhibitors as in the alpha-synuclein aggregation model. We found

197 that both, FCCP and BAPTA-AM, increased the aggregation of Aβ42 (Fig. 4A). BAPTA-AM had

198 a more pronounced effect compared to FCCP, similar to what has been seen for alpha-

199 synuclein aggregation. Inhibition of the Lon protease did not significantly increase Aβ42

200 aggregation, however inhibition of HtrA2 using UCF-101 increased Aβ42 pathology (Fig. 4B).

201 Vice versa, enhancing mitochondrial proteostasis via HtrA2 overexpression decreased Aβ42

202 aggregation, demonstrating that mitochondrial proteostasis plays a role in regulating the

203 aggregation of amyloidogenic proteins (Fig. 4C).

204

205

206 **In-vitro aggregation of Amyloid β 1-42 is influenced by mitochondria and HtrA2**

207

208 In order to show that mitochondria directly influence Aβ42 proteostasis, we analyzed Aβ42

209 aggregation in vitro using a fluorescence lifetime aggregation assay. This assay makes use of

210 the reduction in fluorescence lifetime of labelled proteins when they start to aggregate and

211 are tightly packed, as described in detail by our group before (45, 46). We used Aβ42

212 containing 50 % Hylite^{TM} Fluor 488 labelled Aβ42 which was incubated for 2h at room

213 temperature, showing a reduction of Hylite^{TM} Fluor 488 fluorescence lifetime from 3380 +/-

214 93 ps to 3003 +/- 97 ps within this time interval (Fig. 5A control t0 and t2h). However, in the

215 presence of isolated rat brain mitochondria, only a non-significant drop in Aβ42 Hylite^{TM} Fluor

216 488 fluorescence lifetime occurred (Fig. 5A mito t0 and t2h, 3538 +/- 15 ps compared to 3502

217 +/- 5 ps). Note, the fluorescence lifetime of Aβ42 Hylite^{TM} Fluor 488 incubated with

9

218   mitochondria is higher at the beginning of the experiment (t0) than in the control group (Aβ42

219   + mito 3538 +/- 15 ps compared to Aβ42 control with 3380 +/- 93 ps), since in the control Aβ42

220   starts to aggregate immediately upon preparation. The decrease in Aβ42 Hylite^{TM} Fluor 488

221   fluorescence lifetime seen in the presence of mitochondria was only minor, however, if we

222   pre-incubated mitochondria with UCF-101 Aβ42 Hylite^{TM} Fluor 488 fluorescence lifetime

223   significantly decreased over the 2 h time interval, demonstrating that Aβ42 aggregation is

224   increased upon inhibition of HtrA2 (Fig. 5B, UCF-101 t0 and t2h, 3523 +/- 16 ps compared to

225   3429 +/- 20 ps).

226

227

228   **Inhibition of mitochondrial protein import enhances alpha-synuclein and Amyloid β 1-42**

229   **pathology**

230

231   The effect of mitochondrial proteases on alpha-synuclein and Aβ42 aggregation could just lead

232   to a general mitochondrial dysfunction, however a new line of thinking emerged recently,

233   showing that mitochondrial proteases can influence aggregate dissolution and that

234   aggregation-prone proteins are directed to mitochondrial import (42). There is one report

235   showing mitochondrial import of alpha-synuclein (47), but it is discussed critically that

236   aggregation-prone proteins like alpha-synuclein and Aβ42 are directly imported into

237   mitochondria (48, 49). Thus, in order to prove whether we see alpha-synuclein residing within

238   mitochondria, we immuno-gold labelled YFP-alpha-synuclein in SH-SY5Y cells, and found

239   specific staining within mitochondria, which was mainly located at the inner mitochondrial

240   membrane (Fig. 6A and Supplementary Fig. 2). In addition, we isolated mitochondria from

241   wild-type adult rat brain and probed them for the presence of endogenous alpha-synuclein

242 after protein K (PK) digestion. We saw that alpha-synuclein was still present after PK

243 treatment, indicating that alpha-synuclein resides within the organelle since PK is not able to

244 degrade proteins protected by organelle membranes. This is further supported, since

245 incubation with 0.1% Triton X-100 during PK treatment, which is capable to solubilize

246 mitochondrial membranes (50), enabled complete alpha-synuclein degradation (Fig. 6B and

247 C).

248

249 Since the above results indicate that alpha-synuclein is localized to mitochondria, we

250 hypothesized that inhibition of mitochondrial protein import might have a similar effect on

251 alpha-synuclein pathology as the inhibition of proteases. Thus, using MitobloCK-6, a small

252 molecule inhibitor of protein translocation into mitochondria (51), we equally observed

253 increased alpha-synuclein seeding in YFP-alpha-synuclein SH-SY5Y cells (Fig. 6D). Testing

254 MitobloCK-6 on Aβ42-mCherry overexpressing HEK cells also showed increased aggregation

255 (Fig. 6E), demonstrating that mitochondrial protein import influences the proteostasis of

256 amyloidogenic proteins.

257

258

259 **Discussion**

260

261 The effect of BAPTA-AM on alpha-synuclein seeding took us to study the role of mitochondrial

262 proteostasis on the aggregation of amyloidogenic proteins. We demonstrate here, that

263 inhibition of the mitochondrial proteases HtrA2 and Lon, as well as inhibition of mitochondrial

264 protein import enhances alpha-synuclein pathology. However, downstream effects of

265 mitochondrial dysfunction, induced without mitochondrial integrity disturbance, did not

11

266   recapitulate the increased seeding. Inhibition of HtrA2 as well as inhibition of mitochondrial

267   protein import also increased Aβ42 pathology, and the overexpression of HtrA2 was able to

268   decrease Aβ42 aggregation notably. It was reported recently that mitochondria are able to

269   influence the degradation and protein homeostasis of cytosolic proteins, which was shown in

270   yeast cells upon heat shock (42), however mitochondria may also play an important role for

271   the degradation of amyloidogenic proteins, since mitochondrial proteostasis seems to be

272   clearly coupled to the pathology of alpha-synuclein and Aβ42. HtrA2 appears of particular

273   interest, since it has previously been linked to PD by genetics (52–56) and shows a

274   neuroprotective effect upon overexpression in mice (57, 58).

275

276   So far the effect of amyloid proteins on mitochondria has been interpreted only as a secondary

277   pathological hallmark, with alpha-synuclein as well as Aβ exacerbating mitochondrial

278   dysfunction (48, 49, 59–63). But amyloidogenic proteins might be directed to mitochondrial

279   uptake deliberately, which then disrupts overall mitochondrial function if the uptake is

280   overloaded. So vice versa, an initial failure in mitochondrial function, i.e. by complex I

281   inhibition or upon disturbance of mitophagy, could eventually lead to increased levels of

282   alpha-synuclein, having important implications for sporadic forms of the disease. Our recently

283   published review provides more insights on the mitochondrial uptake of alpha-synuclein and

284   Aβ, on the interaction with mitochondrial translocases as well as background on mitochondrial

285   proteases (64).

286

287   There still remains the argument that inhibition of mitochondrial proteases just causes an

288   unspecific mitochondrial dysfunction which then per se leads to increased alpha-synuclein

289   aggregation. However, it seems that this effect is not mediated via the known downstream

290   events of mitochondrial dysfunction. So it has been shown that ATP depletion is not able to

291   increase alpha-synuclein aggregation, as seen in our study using short term complex I

292   inhibition via MPP^+ reducing ATP without causing major mitochondrial fragmentation and also

293   previously when ATP levels were reduced independently from mitochondrial respiration using

294   2-Desoxyglucose, which inhibits glycolysis (65). Also increased calcium concentrations, when

295   induced acutely via calcium influx through the plasma membrane using the ionophore

296   ionomycin, did not influence alpha-synuclein seeding. This seems to stand in contrast to our

297   previous study (25), where we have shown that calcium affects alpha-synuclein aggregation

298   in-vitro. However, here mainly the nucleation rate was increased, thus calcium may still

299   contribute to PD via alpha-synuclein seed formation. Oxidative stress has been discussed as a

300   likely mechanism, since antioxidants are able to reduce dopaminergic neuron death and

301   alpha-synuclein accumulation after complex I inhibition (65), however also a general

302   protective impact on mitochondria might play a role.

303

304   Though, this does not mean that complex I inhibition, calcium dysregulation and oxidative

305   stress do not play an important role during the course of the disease. Chronic complex I

306   inhibition has clearly been shown to lead to dopaminergic neuron death and alpha-synuclein

307   accumulation (12–16) and is a major factor implicating mitochondrial dysfunction in sporadic

308   Parkinson's disease. Chronic complex I inhibition would lead to reduced mitochondrial fitness

309   and in a similar way high calcium loads do when specific neuronal subtypes are subjected to

310   increased calcium concentrations over long time periods as shown recently for dopaminergic

311   neurons of the substantia nigra (66). Taken together, our study shows that mitochondrial

312   proteostasis may be an important factor in triggering pathology in neurodegeneration and

313   attacking mitochondrial fitness, rather than downstream events of mitochondrial dysfunction

314   might be crucial in the search for therapeutic strategies.

315

316

317   **Material and Methods**

318   ***Human cell culture***

319   *Human neuroblastoma cells* (SH-SY5Y) were obtained from the European Collection of Cell

320   Cultures (ECACC, Sigma-Aldrich, Dorset, UK) and grown in a 1:1 minimal essential medium

321   (MEM) (Sigma-Aldrich) and nutrient mixture F-12 Ham (Sigma-Aldrich) supplemented with 15

322   % FBS, 1 % non-essential amino acids, 2 mM GlutaMAX and 1 % antibiotic-antimycotic (all

323   Thermo Fisher Scientific, Epsom, UK). SH-SY5Y cells stably expressing YFP-alpha-synuclein

324   were obtained by lentiviral transfection using 3rd generation lentiviruses (Addgene constructs:

325   12251, 12253, 12259) (67). Human wild-type alpha-synuclein was inserted into EYFP plasmid

326   (pEYFP-N1) using a 5 amino acid linker (sequence: GCACCGGTCGCCACC) between the C-

327   terminus of alpha-synuclein and N-terminal EYFP. Alpha-synuclein-EYFP was then cloned into

328   the pLJM1 backbone for lentiviral expression (Addgene: 19319) (68). For the preformed fibril

329   (PFF) assay 50,000 cells were plated in MatTek dishes (P35G-1.5-14-C, MatTek Corporation,

330   Ashland, US). For analysis of mitochondrial fragmentation cells were plated at 20,000 per well

331   in NuncTM Lab-TekTM II Chambered Coverglass (8 well, 155409, Thermo Fisher Scientific).

332   Flp-InTM T-RExTM 293 cell line (Invitrogen), a derivative of HEK293 cells containing a stably

333   integrated FRT site and a TetR repressor, were used to generate stable cell lines expressing

334   either mCherry or Aβ42-mCherry (pcDNA3.3-mCherry, pcDNA3.3-Ab42-mCherry) under the

335   Flp-InTM expression vector as described previously (44, 69). Cells were maintained in DMEM

336   high glucose media (Sigma-Aldrich) supplemented with 10% fetal bovine serum (FBS), 2 mM

337   glutaMAX, and 1 % antibiotic-antimycotic (all Thermo Fisher Scientific). Cells were grown at

338   37°C under a 5% CO_2 atmosphere. Cells were plated at 35 000 cells per well in NUNC 24 well

339   plates, and construct expression was induced for 3 days using media above with 1 μg/mL

340   tetracycline (Sigma Aldrich) added. All cell lines were tested for mycoplasma contamination

341   using the MycoAlert™ PLUS mycoplasma detection kit (Lonza, Walkersville). For transient

342   transfection of HtrA2 (70) electroporation with the NEON transfection system was used

343   (settings: 1050 V, 30 ms, 2 pulses; Thermo Fisher Scientific). pcDNA3-HtrA2-FLAG was a gift

344   from L. Miguel Martins (Addgene plasmid # 15938; http://n2t.net/addgene:15938;

345   RRID:Addgene_15938).

346   Cells were imaged on a widefield microscope with IX83 frame (Olympus, Tokyo, Japan),

347   HPLS343 plasma light source (Thorlabs, Newton, US), and Clara interline CCD camera (Andor,

348   Belfast, UK), controlled by Micromanager (71). Respective filter cubes for YFP (excitation 500

349   nm, dichroic mirror 515 nm, emission 535 nm), RFP (excitation 560 nm, dichroic mirror 585

350   nm, emission 630 nm) and DAPI (excitation 350 nm, dichroic mirror 400 nm, emission 460 nm)

351   were used. Images for YFP-alpha-synuclein aggregation and DAPI were taken with an Olympus

352   Plan Apo U 60x/1.42 oil objective lens. Imaging was done randomly by automated acquisition

353   of a grid of 7x7 images per area. Aggregates were identified by their fibrillar nature, cell nuclei

354   were counted using FIJI (72). For Aβ42-mCherry aggregation images were taken with an

355   Olympus LUCPlanFLN 20x/0.45 air objective lens. Aggregates were identified using the

356   Thresholder plugin in ICY (73). The cell surface area was evaluated using the HK-Means plugin

357   for ICY (74).

358

359   ***Alpha-synuclein fibrils***

15

360   Human wild-type (WT) alpha-synuclein was expressed in Escherichia coli One Shot® BL21

361   STAR™ (DE3) (Invitrogen, Thermo Fisher Scientific) cells using plasmid pT7-7 and purified using

362   ion-exchange on a HiPrep Q FF 16/10 anion exchange column (GE Healthcare, Uppsala,

363   Sweden) (75). Alpha-synuclein was then further purified on a HiPrep Phenyl FF 16/10 (High

364   Sub) hydrophobic interaction column (GE Healthcare) (76). Purification was performed on an

365   ÄKTA Pure (GE Healthcare). Monomeric protein was dialyzed against 20 mM phosphate buffer

366   pH 7.2, lyophilized in a LyoQuest 85 freeze-dryer (Telstar, Spain), and stored at -80 °C.

367   Alpha-synuclein fibrils were produced by diluting alpha-synuclein monomer solution to a

368   concentration of 150 µM in 20 mM phosphate buffer, pH 7.2. Samples were incubated at 37°C

369   for 5 days in 0.5 mL Protein Lobind tubes (Eppendorf, Hamburg, Germany) under continuous

370   rotation at maximum speed (UVP HB-1000 Hybridizer, Fisher Scientific). Fibrils were diluted

371   1:1 with 20 mM phosphate buffer, pH 7.2 to a final volume of 200 µL and sonicated (Digital

372   Sonifier® SLPe, model 4C15, Branson, Danbury, USA) with six 10 sec pulses at 70 % amplitude

373   and 10-sec pause after each sonication pulse. Sonicated fibrils were aliquoted, exposed to UV

374   light for 30 min and frozen immediately after at -80C.

375   Alpha-synuclein fibrils were imaged by atomic force microscopy (AFM) (BioScope Catalyst

376   microscope, Bruker AXS GmbH, Fitchburg, USA). Fibrils at an equivalent monomer

377   concentration of 5 µM were deposited for 30 min on High-Performance cover glass (PN

378   474030-9020-000, Carl Zeiss Ltd.), cleaned for 30 min with 1 M KOH (Fluka, Bucharest,

379   Romania) and coated for 30 min with 0.01 % poly-L-Lysine beforehand (P4707, Sigma).

380   Samples were rinsed 5 times with deionized water and dried under nitrogen flow. AFM data

381   were acquired using PeakForce Quantitative Nanomechanical Property mapping mode with

382   ScanAsyst-Fluid+ probes (Bruker AXS GmbH). Images were flattened and exported using

383   NanoScope Analysis software, version 1.8.

384

Preformed fibril (PFF) assay

386 For the induction of alpha-synuclein seeding, YFP-alpha-synuclein overexpressing SH-SY5Y

387 cells were incubated with sonicated preformed alpha-synuclein fibrils as described by Luk et

388 al. (26). Briefly, cells plated in MatTek dishes were washed with Neurobasal medium and

389 subsequently changed to 500 µL Neurobasal medium supplemented with 2 % B27 and 0.5 mM

390 GlutaMAX (all Thermo Fisher Scientific). Cells were preincubated for 1 hour, either using 0.2

391 % DMSO for control or the respective treatment (see cell treatments below). 8 µL of PFFs were

392 diluted with 32 µL HBSS (HBSS minus calcium and magnesium, no phenol red, 14175-053,

393 Thermo Fisher Scientific) and mixed briefly 5 times. Fibrils were added to the bottom of the

394 BioPORTER tube (BioPORTER® Protein Delivery agent, BP502424, Gelantis, San Diego, USA),

395 mixed 5 times and incubated for 5 min at room temperature, then vortexed for 5 sec at 600

396 rpm (Stuart^{TM} Scientific SA8 vortex mixer, Sigma-Aldrich). 460 µL OptiMEM medium (Thermo

397 Fisher Scientific) was added to the BioPORTER tube plus the respective treatments and mixed

398 5 times. The PFF mixture was added dropwise to the cells, settled and then incubated for 4

399 hours at 37°C and 5 % CO_2. Final monomer equivalent concentration of preformed fibrils was

400 600 nM.

401

402 After 4 hours cells were washed twice with 1 ml Neurobasal medium and changed

403 subsequently to 2 mL of retinoic acid medium made of 1:1 minimal essential medium (MEM)

404 (Sigma-Aldrich) and nutrient mixture F-12 Ham (Sigma-Aldrich) supplemented with 5 % FBS, 1

405 % non-essential amino acids, 2 mM GlutaMAX and 1 % antibiotic-antimycotic (all Thermo

406 Fisher Scientific) and 1 µM retinoic acid (Sigma-Aldrich) plus treatments if indicated and

407 incubated for another 3 days to allow aggregate formation. Cells were fixed for 10 min using

408   4 % formaldehyde in PBS supplemented with 4 % sucrose, 5 mM $MgCl_2$ and 10 mM EGTA, pH

409   7.4 (77), stained with Hoechst 33342 (Molecular Probes, Thermo Fisher Scientific) 1:2000 in

410   PBS for 30 min.

411

412   ***Cell treatments***

413   Chemical used for the treatment of cells were prepared as followed, with final dilution made

414   with the respective culture medium. Carbonyl cyanide 4-(trifluoromethoxy)phenylhydrazone

415   (FCCP, Abcam, Cambridge, UK) 1 mM in DMSO, N-Methyl-4-phenylpyridinium Iodide (MPP+,

416   Sigma-Aldrich) 10 mM in water, ionomycin (ab120370, Abcam) 10 mM and 1 mM in DMSO, 2-

417   Deoxyglucose (Sigma-Aldrich) 0.5 M in water, menadione (Sigma-Aldrich) 1.5 mM in DMSO,

418   BAPTA-AM (ab120503, Abcam) 2.5 mM in DMSO, BAPTA (ab144924, Abcam) 1 mM in water,

419   CDDO-Me (Sigma-Aldrich) 1 mM in DMSO, UCF-101 (Sigma-Aldrich) 10 mM in DMSO and

420   MitobloCK-6 (Focus Biomolecules) 5 mM in DMSO.

421

422   ***Immunofluorescence***

423   Cells were fixed as described above, blocking and permeabilisation were performed using 5 %

424   donkey serum in 0.05 % Tween-20 in phosphate-buffered saline (PBS) for 1 h. Primary

425   antibodies were incubated overnight at 4°C, followed by 5 washes with PBS. Secondary

426   antibodies were incubated for 1 hour at room temperature, followed by 5 washes with PBS.

427   As primary antibodies anti-Ubiquitin antibody, clone Apu2 (05-1307, 1:200, Millipore,

428   Watford, United Kingdom), anti-Ubiquitin-binding protein p62, clone 2C11 (SQSTM1, 1:200,

429   Abnova, Taipei, Taiwan) and anti-FLAG® M2 antibody (F1804, 1:200, Sigma-Aldrich) were

430 used. As secondary antibodies anti-rabbit and anti-mouse Alexa Fluor®647, and anti-mouse

431 Alexa Fluor®568 (A-21245, A-21236 and A-11031 from life technologies) were used. Samples

432 were kept in PBS containing 5 mM sodium azide (Sigma-Aldrich).

433

434 ***Structured illumination microscopy (SIM)***

435 Structured illumination images were collected on a custom-built Structured Illumination

436 Microscopy (SIM) setup which has been described in detail (78). A 60×/1.2NA water

437 immersion lens (UPLSAPO 60XW, Olympus) focused the structured illumination pattern onto

438 the sample. This lens also captured the samples' fluorescence emission light before imaging

439 onto a sCMOS camera (C11440, Hamamatsu). Laser excitation wavelengths used were 488 nm

440 (iBEAM-SMART-488, Toptica), 561 nm (OBIS 561, Coherent), and 640 nm (MLD 640, Cobolt).

441 Respective emission filters were BA 510-550 (Olympus), BrightLine FF01-600/37, and

442 BrightLine FF01-676/29 (Semrock, New York, US). Imaging was done in fixed cells or live cells,

443 as indicated. Images were acquired using custom SIM software (HCImage, Mamamatsu

444 Corporation, Sewickley, US). Nine raw images were collected at each plane and each colour.

445 FairSIM plugin in FIJI was used to reconstruct images (79).

446

447 ***FLIM measurements of cytosolic calcium, H_2O_2, and ATP***

448 Fluorescence lifetime microscopy (FLIM) was carried out on a custom-built Time-Correlated

449 Single Photon Counting (TCSPC) system using a super-continuum laser (SC450, Fianium) with

450 a pulse repetition rate of 40 MHz, a confocal scanning unit (FluoView 300, Olympus) coupled

451 with an inverted microscope frame (IX70, Olympus), and a time-correlated single-photon

452 counting system (Becker & Hickl GmbH) as described in detail before (80). The excitation

19

453 wavelength was selected by using an acousto-optic tunable filter (AOTFnC-400.650, Quanta

454 Tech) and respective excitation filters (to improve the wavelength selection), and emission

455 fluorescence was imaged through respective emission filters. The data acquisition time was

456 200s for each FLIM image (10 cycles, 20s per cycle). The photon detection rate was kept below

457 2% of the laser repetition rate in order to avoid photon pile-up.

458 For cytosolic calcium measurements SH-SY5Y cells were incubated with Oregon Green^{TM} 488

459 BAPTA-1, AM (Thermo Fisher Scientific) for 45 min at 1 µM concentration. Excitation was set

460 to 475 nm, excitation filter BrightLine FF01-474/27 (Semrock), and emission filter BrightLine

461 FF01-525/39 (Semrock) were used. For measurement of H_2O_2 and ATP SH-SY5Y cells were

462 transiently transfected with the respective sensor using electroporation with the NEON

463 transfection system (settings: 1100 V, 50 ms, 1 pulse; Thermo Fisher Scientific). HyPer, a

464 genetically encoded sensor consisting of circularly permuted yellow fluorescent protein

465 (cpYFP) inserted into the regulatory domain of the prokaryotic H_2O_2-sensing protein, OxyR

466 (81) was used to measure cytosolic hydrogen peroxide. Excitation was set to 470 nm, same

467 excitation and emission filters as for Oregon Green^{TM} 488 BAPTA-1 were used. Ateam1.03, a

468 FRET-based indicator for ATP composed of the ε subunit of the bacterial F_oF_1-ATP synthase

469 sandwiched by CFP and YFP (82, 83) was used to measure cytosolic ATP levels. Excitation was

470 set to 435 nm, excitation filter BrightLine FF01-434/17 (Semrock), and emission filter

471 BrightLine FF01-470/28 (Semrock) were used. ATeam1.03-nD/nA/pcDNA3 was a gift from

472 Takeharu Nagai (Addgene plasmid # 51958; http://n2t.net/addgene:51958;

473 RRID:Addgene_51958). For ATP measurements cells were subjected to media containing 10

474 mM 2-Deoxyglucose to inhibit glycolysis. The fluorescence lifetime was analyzed by the

475 FLIMfit software tool developed at Imperial College London (84, 85).

476

ThT Assay

The aggregation of alpha-synuclein *in vitro* was measured by Thioflavin T (ThT) assay. Briefly, 50 µL of 100 µM alpha-synuclein with 10 µM fresh ThT added, was incubated for 7 days with 1% DMSO as a control, 10 µM FCCP, 10 µM BAPTA-AM, or 10 µM BAPTA. Assays were performed in NUNC™ black 384-well plates with optical flat bottom (142761, Thermo Fisher Scientific) which were sealed with an Ampliseal transparent microplate sealer (Greiner Bio-One GmbH). Plates were incubated with orbital shaking at 300 rpm for 5 minutes before each read every hour at 37 °C for 170 cycles. The readings of ThT fluorescence intensity were taken using excitation at 440 nm and emission at 480 nm, collected from the bottom up with 20 flashes per well and a gain setting of 1300 (FLUOstar Omega, BMG Labtec GmbH, Ortenberg, Germany). Experiments were repeated three times with four replicates for each condition.

Mitochondrial fragmentation

To label mitochondria SH-SY5Y cells were incubated overnight with 1:1000 CellLight™ Mitochondria-RFP (Thermo Fisher Scientific) and imaged by SIM or a widefield microscope for quantification. Images were taken randomly by automated imaging of a grid, images were analyzed from 3 biological repeats. The mitochondrial length was evaluated using the NIEL Mito algorithm (86, 87).

Animals

Adult female Sprague Dawley rats were supplied by Charles River UK Ltd., Scientific, Breeding and Supplying Establishment, registered under Animals (Scientific Procedures) Act 1986, and AAALAC International accredited. All animal work conformed to guidelines of animal

21

500   husbandry as provided by the UK Home Office. Animals were sacrificed under schedule 1;

501   procedures that do not require specific Home Office approval. Animal work was approved by

502   the NACWO and University of Cambridge Ethics Board.

503

504   ***Mitochondrial isolation and Western blot analysis***

505   Mitochondria were isolated from adult rat brain by differential centrifugation using

506   mitochondria isolation kit for tissue (ab110168, abcam). Western blot for alpha-synuclein was

507   performed using 4–12% Bis-Tris gels (Life Technologies), the protein was transferred onto 0.45

508   µm Millipore PVDF membrane (Fisher Scientific, Loughborough, UK) and subsequently fixed

509   using 4% formaldehyde + 0.1% glutaraldehyde in PBS (both Sigma-Aldrich) (88). As primary

510   antibody α-Synuclein (D37A6) XP® Rabbit mAb was used (1:1000 dilution, #4179, CST, Leiden,

511   Netherlands). An enhanced chemiluminescence (ECL)-horse radish peroxidase (HRP)

512   conjugated secondary antibody (NA934V, 1:1000 dilution, GE Healthcare, Uppsala, Sweden)

513   and SuperSignal West Femto Chemiluminescent Substrate (Thermo Fisher Scientific) were

514   used to probe the membrane, which was exposed using a G:BOX (Syngene, Cambridge, UK).

515   Western blots were analyzed in FIJI (72).

516

517   ***TEM***

518   SH-SY5Y cells and SH-SY5Y cells overexpressing YFP-alpha-synuclein were cultured in 6 well

519   plates (Greiner Bio-One GmbH) at 350 000 per well. After reaching confluency cells were

520   washed with 0.9% NaCl (Sigma-Aldrich) twice and incubated with 8% formaldehyde in 0.05 M

521   sodium cacodylate buffer (Paraformaldehyd from Merck, Darmstadt, Germany) pH 7.4 for 2h

522   at 4°C. Cells were scraped from 6 wells and centrifuged for 10 min at 3500 g. Cells were

523   washed 5 times in 0.05 M sodium cacodylate buffer, 3 times in deionized water, and incubated

524   with 2 % uranyl acetate in 0.05 maleate buffer pH 5.2 (both BDH Chemicals Ltd., Dorset, UK)

525   overnight at 4°C. Cells were washed again and dehydrated at increasing ethanol

526   concentrations (1x 50% EtOH, 3x 70% EtOH, 3x 95 % EtOH, 3x 100% EtOH, 3x 100 % dry EtOH;

527   5 min in each, Sigma-Aldrich). Cells were resuspended in LRW resin (LR White Resin, London

528   Resin (Hard), Agar Scientific, Stansted, UK) mixed 50/50 with dry 100% EtOH and incubated

529   overnight at room temperature. The following day, cells were spun down, and resuspended

530   in pure LRW for 2 days, where LRW was exchanged twice. Cells were centrifuged at 13000 g

531   to form a firm pellet, which was transferred to size 2 gelatine embedding capsules (TAAB,

532   Aldermaston, UK) containing LRW resin. Gelatine capsules were covered with a glass coverslip

533   to exclude any air and the resin was cured at 60°C for 2 days. Gelatine capsules were removed

534   and ultrathin sections were cut using a Leica Ultracut E Ultramicrotome (Leica, Wetzlar,

535   Germany) and placed on 400 mesh nickel/formvar film grids (EM Resolutions). Sections were

536   stained with Anti-GFP antibody (ab6556, Abcam) in blocking solution (2 % BSA (BBITM

537   solutions, Crumlin, UK) in 10 mM TRIS (Sigma-Aldrich) buffer pH 7.4 containing 0.001% Triton-

538   X100 (Calbiochem, San Diego, US) and 0.001% Tween20 (Sigma-Aldrich) at 1:100 overnight.

539   After washing, sections were incubated with goat anti-rabbit 10 nm gold secondary antibody

540   (BBITM solutions) in blocking solution at 1:200 for 1 hour. Sections were washed with washing

541   buffer (same as above omitting BSA), deionized water and left for drying overnight. Post-

542   staining included 2% uranyl acetate in 50 % methanol for 30 sec, followed by washing with 50

543   % methanol and 30-sec staining in Reynold's lead citrate (lead nitrate from BDH Biochemicals

544   Ltd., Trisodiumcitrate from Sigma-Aldrich). Grids were rinsed thoroughly with deionized water

545   and dried before imaging. Grids were imaged on an FEI Tecnai G2 electron microscope

23

546   (Thermo Fisher Scientific) run at 200 keV using a 20 μm objective aperture, images were taken

547   using an AMT V600 camera (AMT, Woburn, US).

548

549   **In-vitro measurements of Aβ42 aggregation**

550   Synthetic Aβ42 and Aβ42 Hilyte™ Fluor 488 (both from Anaspec, Seraing, Belgium) were

551   prepared as previously described (89). Briefly, lyophilized Aβ42 (1 mg) was dissolved in ice-

552   cold trifluroacetic acid (200 mL), sonicated at 0 °C for 60 s and then lyophilized overnight. Ice

553   cold 1,1,1,3,3,3-hexafluro-2-propanol (1 mL) was added, sonicated at 0 °C for 60 s and

554   aliquoted as 20 μL units. The samples were lyophilized overnight and were stored at -80 °C

555   until use. Lyophilized Aβ42 Hilyte™ Fluor 488 peptide (0.1 mg) was dissolved in 1% NH_4OH

556   (200 μL) and sonicated for 60 s at 0 °C. The sample was aliquoted into 5 μL units, snap-frozen

557   in liquid nitrogen and stored at -80 °C. Immediately before the experiment unlabeled Aβ42

558   was prepared by adding first dimethyl sulfoxide (DMSO) (5% of total solvent volume), then

559   sodium phosphate buffer (NaP buffer 50mM, pH 7.4) to reach a concentration of 20 μM. The

560   solution was sonicated at 0 °C for 3 min and centrifuged at 13,400 rpm at 0 °C for 30 min. Then

561   the sample was further diluted to 5 μM concentration with NaP buffer. Also the labelled Aβ42

562   Hilyte™ Fluor 488 was brought to 5 μM concentration in NaP buffer and both were mixed in

563   1:1 ratio. Samples were prepared on ice adding Aβ42, 1 mg/mL of purified mitochondria

564   (preparation see above) and 20 μM UCF-101. Mitochondria isolation buffer and DMSO were

565   added in control samples. 12 μL volume were pipetted in silicon gaskets (Thermo Fisher

566   Scientific, P24742) on a coverslip and measured at room temperature. Fluorescence lifetime

567   measurements (FLIM) were carried out on a custom-built Time-Correlated Single Photon

568   Counting (TCSPC) system as described above (see FLIM measurements of cytosolic calcium,

569   H_2O_2, and ATP).

570

Statistics

572 Statistical analysis was performed using GraphPad Prism 6.07 (GraphPad Software, Inc., La

573 Jolla, CA, USA). Values are given as mean ± SEM unless otherwise stated. Normal distribution

574 was tested using Shapiro-Wilk test. Two-tailed unpaired t-test was used upon normal

575 distribution, two-tailed Mann-Whitney U test was used when no normal distribution was

576 given. For multiple comparisons either one-way ANOVA with Dunnett's post hoc correction

577 upon normal distribution or Kruskal-Wallis test with Dunn's multiple comparison when no

578 normal distribution was given were performed. Significance was considered at $p < 0.05$.

579

Data availability.

581 All relevant data are available from the corresponding authors.

582

583

Acknowledgements

593

Author contributions

J.L., A.F.V. and A.M. contributed to alpha-synuclein PFF assay and cell work. J.L performed

FLIM experiments and mitochondrial morphology analysis. A.D.S. performed alpha-synuclein

in vitro work. J.L. and A.F.V. and C.H. contributed to Western blot analyses. J.L. performed

TEM. J.L., S.W.V. and M.L. contributed to Aβ42 studies. J.M. and M.F. contributed to

automated and SIM imaging. J.L. designed the experiments. J.L., C.F.K. and G.S.K.S. conducted

the overall manuscript.

601

Conflict of interest

The authors declare no conflict of interest.

604

605

References

1.   de Lau, L. M. L., and Breteler, M. M. B. (2006) Epidemiology of Parkinson's disease. *Lancet Neurol*. **5**, 525–535

2.   Polymeropoulos, M. H., Lavedan, C., Leroy, E., Ide, S. E., Dehejia, A., Dutra, A., Pike, B., Root, H., Rubenstein, J., Boyer, R., Stenroos, E. S., Chandrasekharappa, S., Athanassiadou, A., Papapetropoulos, T., Johnson, W. G., Lazzarini, A. M., Duvoisin, R. C., Iorio, G. Di, Golbe, L. I., and Nussbaum, R. L. (1997) Mutation in the α-Synuclein Gene Identified in Families with Parkinson's Disease. *Science (80-.)*. **276**, 2045–2047

3.   Spillantini, M. G., Schmidt, M. L., Lee, V. M., Trojanowski, J. Q., Jakes, R., and Goedert, M. (1997) Alpha-synuclein in Lewy bodies. *Nature*. **388**, 839–840

616   4.   Chartier-Harlin, M., Kachergus, J., Roumier, C., Mouroux, V., Douay, X., and Lincoln, S.

617   (2004) α-synuclein locus duplication as a cause of familial Parkinson's disease. *Lancet*.

618   **364**, 1167–1169

619   5.   Ibáñez, P., Bonnet, a-M., Débarges, B., Lohmann, E., Tison, F., Pollak, P., Agid, Y., Dürr,

620   a, and Brice, a (2004) Causal relation between alpha-synuclein gene duplication and

621   familial Parkinson's disease. *Lancet*. **364**, 1169–1171

622   6.   Singleton, A. B., Farrer, M., Johnson, J., Singleton, A., Hague, S., and Kachergus, J.

623   (2003) α-Synuclein Locus Triplication Causes Parkinson's Disease. *Science (80-.).* **302**,

624   841

625   7.   Goate, A., Chartier-Harlin, M. C., Mullan, M., Brown, J., Crawford, F., Fidani, L., Giuffra,

626   L., Haynes, A., Irving, N., and James, L. (1991) Segregation of a missense mutation in

627   the amyloid precursor protein gene with familial Alzheimer's disease. *Nature*. **349**,

628   704–6

629   8.   Murrell, J., Farlow, M., Ghetti, B., and D, B. M. (1991) A Mutation in the Amyloid

630   Precursor Protein Associated with Hereditary Alzheimer's Disease. *Science (80-.).* **254**,

631   97–99

632   9.   Citron, M., Westaway, D., Xia, W., Carlson, G., Diehl, T., Levesque, G., Johnson-Wood,

633   K., Lee, M., Seubert, P., Davis, A., Kholodenko, D., Motter, R., Sherrington, R., Perry,

634   B., Yao, H., Strome, R., Lieberburg, I., Rommens, J., Kim, S., Schenk, D., Fraser, P., St.

635   George Hyslop, P., and Selkoe, D. J. (1997) Mutant presenilins of Alzheimer's disease

636   increase production of 42-residue amyloid β-protein in both transfected cells and

637   transgenic mice. *Nat. Med.* **3**, 67–72

638   10.   Levy-Lahad, E., Wasco, W., Poorkaj, P., Romano, D. M., Oshima, J., Pettingell, W. H.,

Yu, C., Jondro, P. D., Schmidt, S. D., Wang, K., Crowley, A. C., Fu, Y., Guenette, S. Y., Galas, D., Nemens, E., Wijsman, E. M., Bird, T. D., Schellenberg, G. D., and Tanzi, R. E. (1995) Candidate Gene for the Chromosome 1 Familial Alzheimer 's Disease Locus. *Science (80-.).* **269**, 973–977

11. Sherrington, R., Rogaev, E. I., Liang, Y., Rogaeva, E. A., Levesque, G., Ikeda, M., Chi, H., Lin, C., Li, G., Holman, K., Tsuda, T., Mar, L., Foncin, J. F., Bruni, A. C., Montesi, M. P., Sorbi, S., Rainero, I., Pinessi, L., Nee, L., Chumakov, I., Pollen, D., Brookes, A., Sanseau, P., Polinsky, R. J., Wasco, W., Da Silva, H. A. R., Haines, J. L., Pericak-Vance, M. A., Tanzi, R. E., Roses, A. D., Fraser, P. E., Rommens, J. M., and St George-Hyslop, P. H. (1995) Cloning of a gene bearing missense mutations in early-onset familial Alzheimer's disease. *Nature*. **375**, 754–760

12. Langston, J., Ballard, P., Tetrud, J., and Irwin, I. (1983) Chronic Parkinsonism in humans due to a product of meperidine-analog synthesis. *Science (80-.).* **219**, 979–980

13. Burns, R. S., Chiueh, C. C., Markey, S. P., Ebert, M. H., Jacobowitz, D. M., and Kopin, I. J. (1983) A primate model of parkinsonism: selective destruction of dopaminergic neurons in the pars compacta of the substantia nigra by N-methyl-4-phenyl-1,2,3,6-tetrahydropyridine. *Proc. Natl. Acad. Sci.* **80**, 4546–4550

14. Betarbet, R., Sherer, T. B., Mackenzie, G., Garcia-Osuna, M., Panov, A. V, and Greenamyre, J. T. (2000) Chronic systemic pesticide exposure reproduces features of Parkinson's disease. *Nat. Neurosci.* **3**, 1301–1306

15. Greenamyre, J. T., Sherer, T. B., Betarbet, R., and Panov, a V (2001) Complex I and Parkinson's disease. *IUBMB Life*. **52**, 135–141

16. Sherer, T. B., Kim, J.-H., Betarbet, R., and Greenamyre, J. T. (2003) Subcutaneous

662   Rotenone Exposure Causes Highly Selective Dopaminergic Degeneration and α-

663   Synuclein Aggregation. *Exp. Neurol.* **179**, 9–16

664   17.   Valente, E. M., Abou-Sleiman, P. M., Caputo, V., Muqit, M. M. K., Harvey, K., Gispert,

665   S., Ali, Z., Del Turco, D., Bentivoglio, A. R., Healy, D. G., Albanese, A., Nussbaum, R.,

666   González-Maldonado, R., Deller, T., Salvi, S., Cortelli, P., Gilks, W. P., Latchman, D. S.,

667   Harvey, R. J., Dallapiccola, B., Auburger, G., and Wood, N. W. (2004) Hereditary early-

668   onset Parkinson's disease caused by mutations in PINK1. *Science (80-.).* **304**, 1158–

669   1160

670   18.   Todd, A. M., and Staveley, B. E. (2008) Pink1 suppresses α-synuclein-induced

671   phenotypes in a Drosophila model of Parkinson's disease. *Genome*. **51**, 1040–1046

672   19.   Todd, A. M., and Staveley, B. E. (2012) Expression of Pink1 with α-synuclein in the

673   dopaminergic neurons of Drosophila leads to increases in both lifespan and

674   healthspan. *Genet. Mol. Res.* **11**, 1497–1502

675   20.   Oliveras-Salvá, M., Macchi, F., Coessens, V., Deleersnijder, A., Gérard, M., Van der

676   Perren, A., Van den Haute, C., and Baekelandt, V. (2014) Alpha-synuclein-induced

677   neurodegeneration is exacerbated in PINK1 knockout mice. *Neurobiol. Aging*. **35**,

678   2625–2636

679   21.   Gispert, S., Brehm, N., Weil, J., Seidel, K., Rüb, U., Kern, B., Walter, M., Roeper, J., and

680   Auburger, G. (2015) Potentiation of neurotoxicity in double-mutant mice with Pink1

681   ablation and A53T-SNCA overexpression. *Hum. Mol. Genet.* **24**, 1061–1076

682   22.   Chung, S. Y., Kishinevsky, S., Mazzulli, J. R., Graziotto, J., Mrejeru, A., Mosharov, E. V.,

683   Puspita, L., Valiulahi, P., Sulzer, D., Milner, T. A., Taldone, T., Krainc, D., Studer, L., and

684   Shim, J. won (2016) Parkin and PINK1 Patient iPSC-Derived Midbrain Dopamine

685   Neurons Exhibit Mitochondrial Dysfunction and α-Synuclein Accumulation. *Stem Cell*

686   *Reports*. **7**, 664–677

687   23.   Lu, X.-H., Fleming, S. M., Meurers, B., Ackerson, L. C., Mortazavi, F., Lo, V., Hernandez,

688   D., Sulzer, D., Jackson, G. R., Maidment, N. T., Chesselet, M.-F., and Yang, X. W. (2009)

689   Bacterial Artificial Chromosome Transgenic Mice Expressing a Truncated Mutant

690   Parkin Exhibit Age-Dependent Hypokinetic Motor Deficits, Dopaminergic Neuron

691   Degeneration, and Accumulation of Proteinase K-Resistant alpha-Synuclein. *J.*

692   *Neurosci.* **29**, 1962–1976

693   24.   Creed, R. B., and Goldberg, M. S. (2019) Analysis of α-synuclein pathology in PINK1

694   knockout rat brains. *Front. Neurosci.* **13**, 1–6

695   25.   Lautenschläger, J., Stephens, A. D., Fusco, G., Ströhl, F., Curry, N., Zacharopoulou, M.,

696   Michel, C. H., Laine, R., Nespovitaya, N., Fantham, M., Pinotsi, D., Zago, W., Fraser, P.,

697   Tandon, A., St George-Hyslop, P., Rees, E., Phillips, J. J., De Simone, A., Kaminski, C. F.,

698   and Schierle, G. S. K. (2018) C-terminal calcium binding of α-synuclein modulates

699   synaptic vesicle interaction. *Nat. Commun.* **9**, 712

700   26.   Luk, K. C., Song, C., O'Brien, P., Stieber, A., Branch, J. R., Brunden, K. R., Trojanowski, J.

701   Q., and Lee, V. M.-Y. (2009) Exogenous alpha-synuclein fibrils seed the formation of

702   Lewy body-like intracellular inclusions in cultured cells. *Proc. Natl. Acad. Sci. U. S. A.*

703   **106**, 20051–6

704   27.   Luk, K. C., Kehm, V. M., Zhang, B., O'Brien, P., Trojanowski, J. Q., and Lee, V. M. Y.

705   (2012) Intracerebral inoculation of pathological α-synuclein initiates a rapidly

706   progressive neurodegenerative α-synucleinopathy in mice. *J. Exp. Med.* **209**, 975–86

707   28.   Peelaerts, W., Bousset, L., Van Der Perren, A., Moskalyuk, A., Pulizzi, R., Giugliano, M.,

708   Van Den Haute, C., Melki, R., and Baekelandt, V. (2015) α-Synuclein strains cause

709   distinct synucleinopathies after local and systemic administration. *Nature*. **522**, 340–

710   344

711   29. Pinotsi, D., Michel, C. H., Buell, A. K., Laine, R. F., Mahou, P., Dobson, C. M., Kaminski,

712   C. F., and Kaminski, G. S. (2016) Nanoscopic insights into seeding mechanisms and

713   toxicity of α -synuclein species in neurons. *PNAS*. **113**, 3815–3819

714   30. Thakur, P., Breger, L. S., Lundblad, M., Wan, O. W., Mattsson, B., Luk, K. C., Lee, V. M.

715   Y., Trojanowski, J. Q., and Björklund, A. (2017) Modeling Parkinson's disease

716   pathology by combination of fibril seeds and α-synuclein overexpression in the rat

717   brain. *Proc. Natl. Acad. Sci.* 10.1073/pnas.1710442114

718   31. Follett, J., Darlow, B., Wong, M. B., Goodwin, J., and Pountney, D. L. (2013) Potassium

719   depolarization and raised calcium induces α-synuclein aggregates. *Neurotox. Res.* **23**,

720   378–92

721   32. Friedman, J. R., Lackner, L. L., West, M., DiBenedetto, J. R., Nunnari, J., and Voeltz, G.

722   K. (2011) ER Tubules Mark Sites of Mitochondrial Division. *Science (80-.).* **334**, 358–

723   362

724   33. Criddle, D. N., Gillies, S., Baumgartner-Wilson, H. K., Jaffar, M., Chinje, E. C., Passmore,

725   S., Chvanov, M., Barrow, S., Gerasimenko, O. V., Tepikin, A. V., Sutton, R., and

726   Petersen, O. H. (2006) Menadione-induced reactive oxygen species generation via

727   redox cycling promotes apoptosis of murine pancreatic acinar cells. *J. Biol. Chem.* **281**,

728   40485–40492

729   34. Bajar, B. T., Wang, E. S., Zhang, S., Lin, M. Z., and Chu, J. (2016) A guide to fluorescent

730   protein FRET pairs. *Sensors (Switzerland)*. **16**, 1–24

731   35.   Melo, E. P., Lopes, C., Gollwitzer, P., Lortz, S., Lenzen, S., Mehmeti, I., Kaminski, C. F.,

732   Ron, D., and Avezov, E. (2017) TriPer, an optical probe tuned to the endoplasmic

733   reticulum tracks changes in luminal H2O2. *BMC Biol.* **15**, 1–15

734   36.   Da Cruz, L. N., Alves, E., Leal, M. T., Juliano, M. A., Rosenthal, P. J., Juliano, L., and

735   Garcia, C. R. S. (2011) FRET peptides reveal differential proteolytic activation in

736   intraerythrocytic stages of the malaria parasites Plasmodium berghei and Plasmodium

737   yoelii. *Int. J. Parasitol.* **41**, 363–372

738   37.   Wang, L. F., Christensen, B. N., Bhatnagar, A., and Srivastava, S. K. (2001) Role of

739   calcium-dependent protease(s) in globulization of isolated rat lens cortical fiber cells.

740   *Investig. Ophthalmol. Vis. Sci.* **42**, 194–199

741   38.   Ray, P., Chakrabarti, A. K., Broomfield, C. A., and Ray, R. (2002) Sulfur mustard-

742   stimulated protease: A target for antivesicant drugs. *J. Appl. Toxicol.* **22**, 139–140

743   39.   Demartino, G. N., Croall, D. E., and Calcium-dependent, D. E. (1982) Calcium-

744   Dependent Proteases in Neuroblastoma Cells. *J. Neurochem.* **38**, 1642–1648

745   40.   Mellgren, L. (1987) Calcium-dependent proteases: an enzyme system active at cellular

746   membranes? *FASEB J*. **1**, 110–5

747   41.   Gibellini, L., Pinti, M., Bartolomeo, R., De Biasi, S., Cormio, A., Musicco, C., Carnevale,

748   G., Pecorini, S., Nasi, M., De Pol, A., and Cossarizza, A. (2015) Inhibition of Lon

749   protease by triterpenoids alters mitochondria and is associated to cell death in human

750   cancer cells. *Oncotarget*. **6**, 25466–83

751   42.   Ruan, L., Zhou, C., Jin, E., Kucharavy, A., Zhang, Y., Wen, Z., Florens, L., and Li, R.

752   (2017) Cytosolic proteostasis through importing of misfolded proteins into

753   mitochondria. *Nature*. **543**, 443–446

754   43.   Cilenti, L., Lee, Y., Hess, S., Srinivasula, S., Park, K. M., Junqueira, D., Davis, H.,

755   Bonventre, J. V., Alnemri, E. S., and Zervos, A. S. (2003) Characterization of a novel and

756   specific inhibitor for the pro-apoptotic protease Omi/HtrA2. *J. Biol. Chem.* **278**,

757   11489–11494

758   44.   Lu, M., Williamson, N., Mishra, A., Michel, C. H., Kaminski, C. F., Tunnacliffe, X. A., and

759   Schierle, X. G. S. K. (2019) Structural progression of amyloid-beta Arctic mutant

760   aggregation in cells revealed by multiparametric imaging. *J. Biol. Chem.* **294**, 1478–

761   1487

762   45.   Chen, W., Young, L. J., Lu, M., Zaccone, A., Strohl, F., Yu, N., Schierle, G. S. K., and

763   Kaminski, C. F. (2017) Fluorescence self-quenching from reporter dyes informs on the

764   structural properties of amyloid clusters formed in vitro and in cells. *Nano Lett.* **17**,

765   143–149

766   46.   Kaminski Schierle, G. S., Bertoncini, C. W., Chan, F. T. S., Van Der Goot, A. T.,

767   Schwedler, S., Skepper, J., Schlachter, S., Van Ham, T., Esposito, A., Kumita, J. R.,

768   Nollen, E. A. A., Dobson, C. M., and Kaminski, C. F. (2011) A FRET sensor for non-

769   invasive imaging of amyloid formation in vivo. *ChemPhysChem*. **12**, 673–680

770   47.   Devi, L., Raghavendran, V., Prabhu, B. M., Avadhani, N. G., and

771   Anandatheerthavarada, H. K. (2008) Mitochondrial import and accumulation of α-

772   synuclein impair complex I in human dopaminergic neuronal cultures and Parkinson

773   disease brain. *J. Biol. Chem.* **283**, 9089–9100

774   48.   Cenini, G., Rub, C., Bruderek, M., and Voos, W. (2016) Amyloid β-peptides interfere

775   with mitochondrial preprotein import competence by a coaggregation process. *Mol.*

776   *Biol. Cell*. **27**, 3257–3272

33

777   49.   Di Maio, R., Barrett, P. J., Hoffman, E. K., Barrett, C. W., Zharikov, A., Borah, A., Hu, X.,

778   McCoy, J., Chu, C. T., Burton, E. A., Hastings, T. G., and Greenamyre, J. T. (2016) α-

779   synuclein binds to TOM20 and inhibits mitochondrial protein import in Parkinson's

780   disease. *Sci. Transl. Med.* **8**, 1–14

781   50.   Gurtubay, J. I. G., Goñi, F. M., Gómez-Fernández, J. C., Otamendi, J. J., and Macarulla,

782   J. M. (1980) Triton X-100 solubilization of mitochondrial inner and outer membranes.

783   *J. Bioenerg. Biomembr.* **12**, 47–70

784   51.   Dabir, D. V., Hasson, S. A., Setoguchi, K., Johnson, M. E., Wongkongkathep, P.,

785   Douglas, C. J., Zimmerman, J., Damoiseaux, R., Teitell, M. A., and Koehler, C. M. (2013)

786   A small molecule inhibitor of redox-regulated protein translocation into mitochondria.

787   *Dev. Cell*. **25**, 81–92

788   52.   Strauss, K. M., Martins, L. M., Plun-Favreau, H., Marx, F. P., Kautzmann, S., Berg, D.,

789   Gasser, T., Wszolek, Z., Müller, T., Bornemann, A., Wolburg, H., Downward, J., Riess,

790   O., Schulz, J. B., and Krüger, R. (2005) Loss of function mutations in the gene encoding

791   Omi/HtrA2 in Parkinson's disease. *Hum. Mol. Genet.* **14**, 2099–2111

792   53.   Bogaerts, V., Nuytemans, K., Reumers, J., Pals, P., Engelborghs, S., Pickut, B., Corsmit,

793   E., Peeters, K., Schymkowitz, J., De Deyn, P. P., Cras, P., Rousseau, F., Theuns, J., and

794   Van Broeckhoven, C. (2008) Genetic variability in the mitochondrial serine protease

795   HTRA2 contributes to risk for Parkinson disease. *Hum. Mutat.* **29**, 832–840

796   54.   Westerlund, M., Behbahani, H., Gellhaar, S., Forsell, C., Belin, A. C., Anvret, A.,

797   Zettergren, A., Nissbrandt, H., Lind, C., Sydow, O., Graff, C., Olson, L., Ankarcrona, M.,

798   and Galter, D. (2011) Altered enzymatic activity and allele frequency of OMI/HTRA2 in

799   Alzheimer's disease. *FASEB J.* **25**, 1345–52

800   55.   Unal Gulsuner, H., Gulsuner, S., Mercan, F. N., Onat, O. E., Walsh, T., Shahin, H., Lee,

801   M. K., Dogu, O., Kansu, T., Topaloglu, H., Elibol, B., Akbostanci, C., King, M.-C., Ozcelik,

802   T., and Tekinay, A. B. (2014) Mitochondrial serine protease HTRA2 p.G399S in a

803   kindred with essential tremor and Parkinson disease. *Proc. Natl. Acad. Sci.* **111**,

804   18285–18290

805   56.   Chao, Y. X., Ng, E. Y., Foo, J. N., Liu, J., Zhao, Y., and Tan, E. K. (2015) Mitochondrial

806   serine protease HTRA2 gene mutation in Asians with coexistent essential tremor and

807   Parkinson disease. *Neurogenetics*. **16**, 241–242

808   57.   Jones, J. M., Datta, P., Srinivasula, S. M., Ji, W., Gupta, S., Zhang, Z. J., Davies, E.,

809   Hajnóczky, G., Saunders, T. L., Van Keuren, M. L., Fernandes-Alnemri, T., Meisler, M.

810   H., and Alnemri, E. S. (2003) Loss of Omi mitochondrial protease activity causes the

811   neuromuscular disorder of mnd2 mutant mice. *Nature*. **425**, 721–727

812   58.   Martins, L. M., Morrison, A., Klupsch, K., Fedele, V., Moisoi, N., Teismann, P., Abuin,

813   A., Grau, E., Geppert, M., George, P., Creasy, C. L., Martin, A., Hargreaves, I., Heales, S.

814   J., Okada, H., Brandner, S., Schulz, B., Mak, T., Downward, J., and Livi, G. P. (2004)

815   Neuroprotective Role of the Reaper-Related Serine Protease HtrA2 / Omi Revealed by

816   Targeted Deletion in Mice. *Mol. Cell. Biol.* **24**, 9848–9862

817   59.   Anandatheerthavarada, H. K., Biswas, G., Robin, M. A., and Avadhani, N. G. (2003)

818   Mitochondrial targeting and a novel transmembrane arrest of Alzheimer's amyloid

819   precursor protein impairs mitochondrial function in neuronal cells. *J. Cell Biol.* **161**,

820   41–54

821   60.   Devi, L. (2006) Accumulation of Amyloid Precursor Protein in the Mitochondrial

822   Import Channels of Human Alzheimer's Disease Brain Is Associated with Mitochondrial

823   Dysfunction. *J. Neurosci.* **26**, 9057–9068

824   61.   Mossmann, D., Vögtle, F. N., Taskin, A. A., Teixeira, P. F., Ring, J., Burkhart, J. M.,

825   Burger, N., Pinho, C. M., Tadic, J., Loreth, D., Graff, C., Metzger, F., Sickmann, A., Kretz,

826   O., Wiedemann, N., Zahedi, R. P., Madeo, F., Glaser, E., and Meisinger, C. (2014)

827   Amyloid-β peptide induces mitochondrial dysfunction by inhibition of preprotein

828   maturation. *Cell Metab.* **20**, 662–669

829   62.   Rui, Y., and Zheng, J. Q. (2016) Amyloid β oligomers elicit mitochondrial transport

830   defects and fragmentation in a time-dependent and pathway-specific manner. *Mol.*

831   *Brain*. **9**, 79

832   63.   Subramaniam, S. R., Vergnes, L., Franich, N. R., Reue, K., and Chesselet, M. F. (2014)

833   Region specific mitochondrial impairment in mice with widespread overexpression of

834   alpha-synuclein. *Neurobiol. Dis.* **70**, 204–213

835   64.   Lautenschäger, J., and Kaminski Schierle, G. S. (2019) Mitochondrial degradation of

836   amyloidogenic proteins — A new perspective for neurodegenerative diseases. *Prog.*

837   *Neurobiol.* **181**, 101660

838   65.   Sherer, T. B., Betarbet, R., Testa, C. M., Seo, B. B., Richardson, J. R., Kim, J. H., Miller,

839   G. W., Yagi, T., Matsuno-Yagi, A., and Greenamyre, J. T. (2003) Mechanism of toxicity

840   in rotenone models of Parkinson's disease. *J Neurosci*. **23**, 10756–10764

841   66.   Guzman, J. N., Ilijic, E., Yang, B., Sanchez-Padilla, J., Wokosin, D., Galtieri, D.,

842   Kondapalli, J., Schumacker, P. T., and Surmeier, D. J. (2018) Systemic isradipine

843   treatment diminishes calcium-dependent mitochondrial oxidant stress. *J. Clin. Invest.*

844   10.1172/JCI95898

845   67.   Dull, T., Zufferey, R., Kelly, M., Mandel, R. J., Nguyen, M., Trono, D., and Naldini, L.

846   (1998) A third-generation lentivirus vector with a conditional packaging system. *J.*

847   *Virol.* **72**, 8463–71

848   68.   Sancak, Y., Peterson, T. R., Shaul, Y. D., Lindquist, R. A., Thoreen, C. C., Bar-Peled, L.,

849   and Sabatini, D. M. (2008) The rag GTPases bind raptor and mediate amino acid

850   signaling to mTORC1. *Science (80-.).* **320**, 1496–1501

851   69.   Wu, H., Zhang, F., Williamson, N., Jian, J., Zhang, L., Liang, Z., Wang, J., An, L.,

852   Tunnacliffe, A., and Zheng, Y. (2014) Effects of secondary metabolite extract from

853   Phomopsis occultaon β-amyloid aggregation. *PLoS One*.

854   10.1371/journal.pone.0109438

855   70.   Plun-Favreau, H., Klupsch, K., Moisoi, N., Gandhi, S., Kjaer, S., Frith, D., Harvey, K.,

856   Deas, E., Harvey, R. J., McDonald, N., Wood, N. W., Martins, L. M., and Downward, J.

857   (2007) The mitochondrial protease HtrA2 is regulated by Parkinson's disease-

858   associated kinase PINK1. *Nat. Cell Biol.* **9**, 1243–1252

859   71.   Edelstein, A. D., Tsuchida, M. A., Amodaj, N., Pinkard, H., Vale, R. D., and Stuurman, N.

860   (2014) Advanced methods of microscope control using µManager software. *J. Biol.*

861   *Methods*. **1**, 10

862   72.   Schindelin, J., Arganda-Carreras, I., Frise, E., Kaynig, V., Longair, M., Pietzsch, T.,

863   Preibisch, S., Rueden, C., Saalfeld, S., Schmid, B., Tinevez, J.-Y., White, D. J.,

864   Hartenstein, V., Eliceiri, K., Tomancak, P., and Cardona, A. (2012) Fiji: an open-source

865   platform for biological-image analysis. *Nat. Methods*. **9**, 676–682

866   73.   de Chaumont, F., Dallongeville, S., Chenouard, N., Hervé, N., Pop, S., Provoost, T.,

867   Meas-Yedid, V., Pankajakshan, P., Lecomte, T., Le Montagner, Y., Lagache, T., Dufour,

868   A., and Olivo-Marin, J.-C. (2012) Icy: an open bioimage informatics platform for

869   extended reproducible research. *Nat. Methods*. **9**, 690–696

870   74.   Arai, K., and Barakbah, A. R. (2007) Hierarchical K-means: an algorithm for centroids

871   initialization for K-means. *Rep. Fac. Sci. Engrg. Reports Fac. Sci. Eng. Saga Univ. Saga*

872   *Univ.* **36**, 36–125

873   75.   Huang, C., Ren, G., Zhou, H., and Wang, C. (2005) A new method for purification of

874   recombinant human alpha-synuclein in Escherichia coli. *Protein Expr. Purif.* **42**, 173–

875   177

876   76.   Campioni, S., Carret, G., Jordens, S., Ce Nicoud, L., Mezzenga, R., and Riek, R. (2014)

877   The Presence of an Air–Water Interface Affects Formation and Elongation of α‑

878   Synuclein Fibrils. 10.1021/ja412105t

879   77.   Marchenko, S., and Flanagan, L. (2007) Immunocytochemistry: human neural stem

880   cells. *J. Vis. Exp.* 10.3791/267

881   78.   Young, L. J., Ströhl, F., and Kaminski, C. F. (2016) A Guide to Structured Illumination

882   TIRF Microscopy at High Speed with Multiple Colors. *J. Vis. Exp.* 10.3791/53988

883   79.   Müller, M., Mönkemöller, V., Hennig, S., Hübner, W., and Huser, T. (2016) Open-

884   source image reconstruction of super-resolution structured illumination microscopy

885   data in ImageJ. *Nat. Commun.* **7**, 1–6

886   80.   Chen, W. Y., Avezov, E., Schlachter, S. C., Gielen, F., Laine, R. F., Harding, H. P.,

887   Hollfelder, F., Ron, D., and Kaminski, C. F. (2015) A method to quantify FRET

888   stoichiometry with phasor plot analysis and acceptor lifetime ingrowth. *Biophys. J.*

889   **108**, 999–1002

890   81.   Belousov, V. V, Fradkov, A. F., Lukyanov, K. A., Staroverov, D. B., Shakhbazov, K. S.,

891   Terskikh, A. V, and Lukyanov, S. (2006) Genetically encoded fluorescent indicator for

892   intracellular hydrogen peroxide. *Nat. Methods*. **3**, 281–286

893 82. Imamura, H., Nhat, K. P. H., Togawa, H., Saito, K., Iino, R., Kato-Yamada, Y., Nagai, T.,

894   and Noji, H. (2009) Visualization of ATP levels inside single living cells with

895   fluorescence resonance energy transfer-based genetically encoded indicators. *Proc.*

896   *Natl. Acad. Sci. U. S. A.* **106**, 15651–15656

897 83. Kotera, I., Iwasaki, T., Imamura, H., Noji, H., and Nagai, T. (2010) Reversible

898   Dimerization of Aequorea victoria Fluorescent Proteins Increases the Dynamic Range

899   of FRET-Based Indicators. *ACS Chem. Biol.* **5**, 321–332

900 84. Görlitz, F., Kelly, D. J., Warren, S. C., Alibhai, D., West, L., Kumar, S., Alexandrov, Y.,

901   Munro, I., Garcia, E., McGinty, J., Talbot, C., Serwa, R. A., Thinon, E., da Paola, V.,

902   Murray, E. J., Stuhmeier, F., Neil, M. A. A., Tate, E. W., Dunsby, C., and French, P. M.

903   W. (2017) Open Source High Content Analysis Utilizing Automated Fluorescence

904   Lifetime Imaging Microscopy. *J. Vis. Exp.* 10.3791/55119

905 85. Warren, S. C., Margineanu, A., Alibhai, D., Kelly, D. J., Talbot, C., Alexandrov, Y.,

906   Munro, I., Katan, M., Dunsby, C., and French, P. M. W. (2013) Rapid Global Fitting of

907   Large Fluorescence Lifetime Imaging Microscopy Datasets. *PLoS One*.

908   10.1371/journal.pone.0070687

909 86. Lautenschläger, J., Lautenschläger, C., Tadic, V., Suesse, H., Ortmann, W., Denzler, J.,

910   Stallmach, A., Witte, O. W., and Grosskreutz, J. (2015) Novel computer vision

911   algorithm for the reliable analysis of organelle morphology in whole cell 3D images - A

912   pilot study for the quantitative evaluation of mitochondrial fragmentation in

913   amyotrophic lateral sclerosis. *Mitochondrion*. **25**, 49–59

87. Herbert, S., Ortmann, W., Lautenschl, J., Marco, K., Grosskreutz, J., and Denzler, J. (2014) Quantitative Analysis of Pathological Mitochondrial Morphology in Neuronal Cells in Confocal Laser Scanning Microscopy Images. *Proc. IWBBIO*

88. Lee, B. R., and Kamitani, T. (2011) Improved immunodetection of endogenous α-synuclein. *PLoS One*. **6**, e23939

89. Sum, T. H., Sum, T. J., Galloway, W. R. J. D., Collins, S., Twigg, D. G., Hollfelder, F., and Spring, D. R. (2016) Combinatorial synthesis of structurally diverse triazole-bridged flavonoid dimers and trimers. *Molecules*. 10.3390/molecules21091230

Figure Legends

Fig. 1. BAPTA-AM increases alpha-synuclein pathology.

(A) YFP-alpha-synuclein SH-SY5Y cells were treated with DMSO (control), 10 µM BAPTA-AM for 1h (before fibrillar seed incubation) and for 5h (before plus during the incubation with alpha-synuclein fibrillar seeds). Scale bars: 20 µm. Alpha-synuclein seeding was increased upon 1h pre-treatment and 5h treatment with BAPTA-AM. Data are presented as mean ± SEM. *p = 0.0127 and ****p < 0.0001 (Kruskal-Wallis test with Dunn's multiple comparison). N = 16, 9, 15 with n = regions analyzed, three biological repeats.

(B) Fluorescence lifetime images of cytosolic calcium levels (Oregon Green™ 488 BAPTA-1 fluorescence lifetime) in SH-SY5Y cells treated with DMSO (control), 10 µM BAPTA-AM for 10 min, 1h or 5h. The cytosolic calcium level within cells was significantly reduced upon 10 min incubation with BAPTA-AM, however after 1h of incubation with BAPTA-AM calcium levels

937   returned back to basal levels. After 5h treatment with BAPTA-AM calcium levels significantly

938   increased beyond basal calcium levels. Data are presented as mean ± SEM. ****p < 0.0001

939   (Kruskal-Wallis test with Dunn's multiple comparison). N = 88, 54, 61, 46, with n = cells

940   analyzed, three biological repeats.

941   (C) ThT assay displaying the aggregation kinetics of alpha-synuclein in-vitro in the presence of

942   DMSO, 10 µM BAPTA-AM, or 10 µM BAPTA. Data are presented from three biological repeats.

943   (D) Mito-RFP stained mitochondrial network in SH-SH5Y cells. Cells were treated with DMSO

944   (control) or 10 µM BAPTA-AM for 5h. Scale bars: 5 µm.

945   (E) YFP-alpha-synuclein SH-SY5Y cells treated with DMSO (control), 10 µM FCCP for 1h (before

946   fibrillar seed incubation) and for 5h (before plus during the incubation with alpha-synuclein

947   fibrillar seeds). Scale bars: 20 µm. Alpha-synuclein seeding was increased upon 5h treatment

948   with FCCP. Data are presented as mean ± SEM. **p = 0.0064 (Kruskal-Wallis test with Dunn's

949   multiple comparison). N = 16, 6, 9 with n = regions analyzed, three biological repeats.

950   (F) ThT assay displaying the aggregation kinetics of alpha-synuclein in-vitro in the presence of

951   DMSO or 10 µM FCCP. Data are presented from three biological repeats.

952

953   **Fig. 2. Downstream effectors of mitochondrial dysfunction do not influence alpha-synuclein**

954   **pathology.**

955   (A) YFP-alpha-synuclein SH-SY5Y cells were treated with DMSO (control), 500 µM MPP[+], 1 µM

956   ionomycin, or 3 µM menadione for 3 days (1h before, during alpha-synuclein fibrillar seed

957   incubation, and during the 3 day period until evaluation). Scale bars: 20 µm. Alpha-synuclein

958   seeding was not significantly increased (one-way ANOVA with Dunnett's post-hoc correction).

959   Data are presented as mean ± SEM, N = 11, 8, 8, 7 with n = regions analyzed, three biological

960   repeats.

961 (B) Fluorescence lifetime images and graphs for ATP levels (Ateam1.03 fluorescence lifetime)

962 in SH-SY5Y cells treated with DMSO (control), 500 µM MPP+, 10 µM FCCP and 10 µM BAPTA-

963 AM for 1h. The effect of 500 µM MPP+ and FCCP was significant, BAPTA-AM had no significant

964 effect. ****$p < 0.0001$ and N = 43, 74, 48, 47.

965 (C) Fluorescence lifetime images and graphs for cytosolic calcium levels (Oregon Green™ 488

966 BAPTA-1 fluorescence lifetime) in SH-SY5Y cells treated with DMSO (control), 1 µM ionomycin,

967 10 µM FCCP and 10 µM BAPTA-AM for 1h. The effect of 1 µM ionomycin and FCCP was

968 significant. Both, the effect of FCCP and BAPTA-AM treatment were lower than seen with

969 ionomycin. ****$p < 0.0001$ and N = 88, 60, 42, 61.

970 (D) Fluorescence lifetime images and graphs of H_2O_2 levels (HyPer fluorescence lifetime) in

971 SH-SY5Y cells treated with DMSO (control), 3 µM menadione, 10 µM FCCP and 10 µM BAPTA-

972 AM for 1h. The effect of 3 µM menadione, FCCP and BAPTA-AM was significant. Both, FCCP

973 and BAPTA-AM did not produce a higher effect than seen with menadione. **$p = 0.0017$, $p =$

974 0.0012 and $p = 0.0058$ and N = 79, 63, 36, 70. All scale bars: 20 µm. Data are presented as

975 mean ± SEM with n = cells analyzed, Kruskal-Wallis test with Dunn's multiple comparison,

976 three biological repeats.

977

978 **Fig. 3. Inhibition of mitochondrial proteases increases alpha-synuclein pathology.**

979 (A and B) Quantification of mitochondrial fragmentation after 5h treatment with 10 µM FCCP,

980 10 µM BAPTA-AM, 500 µM MPP+, 1 µM ionomycin and 3 µM menadione. The mitochondrial

981 length was significantly decreased after treatment with FCCP and BAPTA-AM. Scale bars: 10

982 µm. Data are presented as mean ± SEM. ****$p < 0.0001$ (Kruskal-Wallis test with Dunn's

983 multiple comparison). N = 76, 92, 103, 90, 88, 89 with n = individual images, three biological

984 repeats. Images analysis of mitochondrial fragmentation was performed using NIEL Mito (86),

985   (C) YFP-alpha-synuclein SH-SY5Y cells were treated with DMSO (control), 1 μM CDDO-Me, or

986   20 μM UCF-101 before and during the incubation with alpha-synuclein fibrillar seeds (5h).

987   Scale bars: 20 μm. Alpha-synuclein seeding was increased upon both treatments. Data are

988   presented as mean ± SEM. **p = 0.005 and ****p < 0.0001 (Kruskal-Wallis test with Dunn's

989   multiple comparison). N = 15, 9, 11 with n = regions analyzed, three biological repeats.

990

991   **Fig. 4. Mitochondrial proteostasis influences Amyloid β 1-42 pathology.**

992   (A) Aβ42-mCherry overexpressing HEK cells were treated with DMSO (control), 1 μM FCCP or

993   10 μM BAPTA-AM for 24 h. The aggregation of Aβ42 was increased upon treatment with FCCP

994   and BAPTA-AM. Data are presented as mean ± SEM. *p = 0.0298 and ****p < 0.0001 (Kruskal-

995   Wallis test with Dunn's multiple comparison). N = 9, for all conditions, with n = wells analyzed,

996   three biological repeats.

997   (B) Aβ42-mCherry cells were treated with DMSO (control), 0.1 μM CDDO-Me or 20 μM UCF-

998   101 for 24 h. The aggregation of Aβ42 was increased upon treatment with UCF-101. Data are

999   presented as mean ± SEM. ***p = 0.0001 (one-way ANOVA with Dunnett's post-hoc

1000   correction). N = 9, for all conditions, with n = wells analyzed, three biological repeats.

1001   (C) Aβ42-mCherry cells were transfected with either uncut pcDNA3 (control) or HtrA2 pcDNA3

1002   and Aβ42-mCherry expression was induced with tetracycline for 3 days. The aggregation of

1003   Aβ42 was significantly decreased upon overexpression of HtrA2. Data are presented as mean

1004   ± SEM. **p = 0.0089 (two-tailed unpaired t-test). N = 9, 9 with n = regions analyzed, three

1005   biological repeats. Scale bars: 20 μm.

1006

1007   **Fig. 5. HtrA2 influences in-vitro aggregation of Aβ42.**

1008 (A) Fluorescence lifetime images of Hilyte™ Fluor 488 labelled Aβ42 at the beginning of the

1009 experiment (t0) and after 2 h of incubation at room temperature (t2h) show a decrease in

1010 fluorescence lifetime in control conditions demonstrating protein aggregation. No decrease

1011 in Aβ42 Hilyte™ Fluor 488 fluorescence lifetime was seen upon addition of isolated

1012 mitochondria. Data are presented as mean ± SEM. **p =0.0025 and ****p< 0.0001 (one-way

1013 ANOVA with Tukey's post-hoc correction). N = 7, 8, 7, 7 with n = wells analyzed, three

1014 biological repeats. Scale bars: 20 µm.

1015 (B) Fluorescence lifetime images of Hilyte™ Fluor 488 labelled Aβ42 at the beginning of the

1016 experiment (t0) and after 2 h of incubation at room temperature (t2h), showing a decrease in

1017 the Aβ42 Hilyte™ Fluor 488 fluorescence lifetime when UCF-101 treated mitochondria were

1018 added. Data are presented as mean ± SEM. ***p =0.0009 and *p= 0.0142 (one-way ANOVA

1019 with Tukey's post-hoc correction). N = 8, 8, 7, 8 with n = wells analyzed, three biological

1020 repeats. Scale bars: 20 µm.

1021

1022 **Fig. 6. Inhibition of mitochondrial protein import increases alpha-synuclein and Aβ42**

1023 **pathology.**

1024 (A) Transmission electron microscopy (TEM) image of immunogold labelled YFP-alpha-

1025 synuclein in SH-SY5Y cells showing that alpha-synuclein is contained within mitochondria.

1026 Arrows indicate individual immunogold labels within mitochondria. m = mitochondria, cyt =

1027 cytoplasm. Scale bar: 100 nm.

1028 (B) Alpha-synuclein of isolated mitochondria from adult rat brain in the absence (native) of

1029 proteinase K (PK), in the presence of PK or in the presence of both PK and 0.1% TritonX-100.

1030 (C) Relative intensity of alpha-synuclein bands normalized to native mitochondria. Data are

1031 presented as mean ± SEM. ***p = 0.0007, ****p = < 0.0001, **p = 0.0017 (one-way ANOVA

1032 with Tukey's post-hoc correction). N = 3 for all conditions with n = biological repeats.

1033 (D) YFP-alpha-synuclein SH-SY5Y were cells treated with DMSO (control), or 50 µM MitobloCK-

1034 6 before and during the incubation with alpha-synuclein fibrillar seeds (5h). Scale bars: 20 µm.

1035 Alpha-synuclein seeding was significantly increased upon treatment. Data are presented as

1036 mean ± SEM. ****p < 0.0001 (two-tailed Mann-Whitney U test). N = 15, 11 with n = regions

1037 analyzed, three biological repeats.

1038 (E) Aβ42-mCherry cells were treated with DMSO (control) or 5 µM MitobloCK-6 for 24 h. The

1039 aggregation of Aβ42 was increased upon treatment with MitobloCK-6. Data are presented as

1040 mean ± SEM. **p = 0.0088 (two-tailed unpaired t-test). N = 9, for all conditions, with n = wells

1041 analyzed, three biological repeats.

1042

1043

1044 **Supplementary Fig. 1. Incubation of SH-SY5Y cells overexpressing YFP-alpha-synuclein with**

1045 **alpha-synuclein seeds leads to YFP-alpha-synuclein fibril formation.**

1046 (A) Schematic overview of the cellular alpha-synuclein aggregation assay.

1047 (B) Fibrillar seeds generated from recombinant human wild-type alpha-synuclein shown by

1048 atomic force microscopy before (upper panel) and after sonication (lower panel). Scale bars:

1049 1 µm.

1050 (C) Structured illumination microscopy (SIM) images of SH-SY5Y cells overexpressing YFP-

1051 tagged alpha-synuclein in the absence (left) and upon incubation with alpha-synuclein fibrillar

1052 seeds (right). Scale bars: 10 µm.

1053   (D and E) Co-staining of YFP-alpha-synuclein fibrillar aggregates with ubiquitin and ubiquitin-

1054   binding protein p62. Scale bars: 10 μm.

1055

1056   **Supplementary Fig. 2. TEM of immunogold labelled YFP-alpha-synuclein, supplementary to**

1057   **Fig. 6A.**

1058   (A) Representative images of transmission electron microscopy (TEM) from SH-SY5Y cells

1059   overexpressing YFP-alpha-synuclein showing that alpha-synuclein is contained within

1060   mitochondria. Arrows indicate individual immunogold labelling within mitochondria. Scale

1061   bars: 100 nm small images, 500 nm large overview image.

1062   (B) TEM images and quantification of anti-GFP staining in control SH-SY5Y cells and SH-SY5Y

1063   cells overexpressing YFP-alpha-synuclein. Quantification of gold particles / μm^2 shows that the

1064   staining is enriched in YFP-alpha-synuclein overexpressing cells and not due to unspecific

1065   background. Data are presented as mean ± SEM. ***p = 0.0002 (two-tailed unpaired t-test).

1066   N = 10, 13 with n = images analyzed. Scale bars: 500 nm.

1067

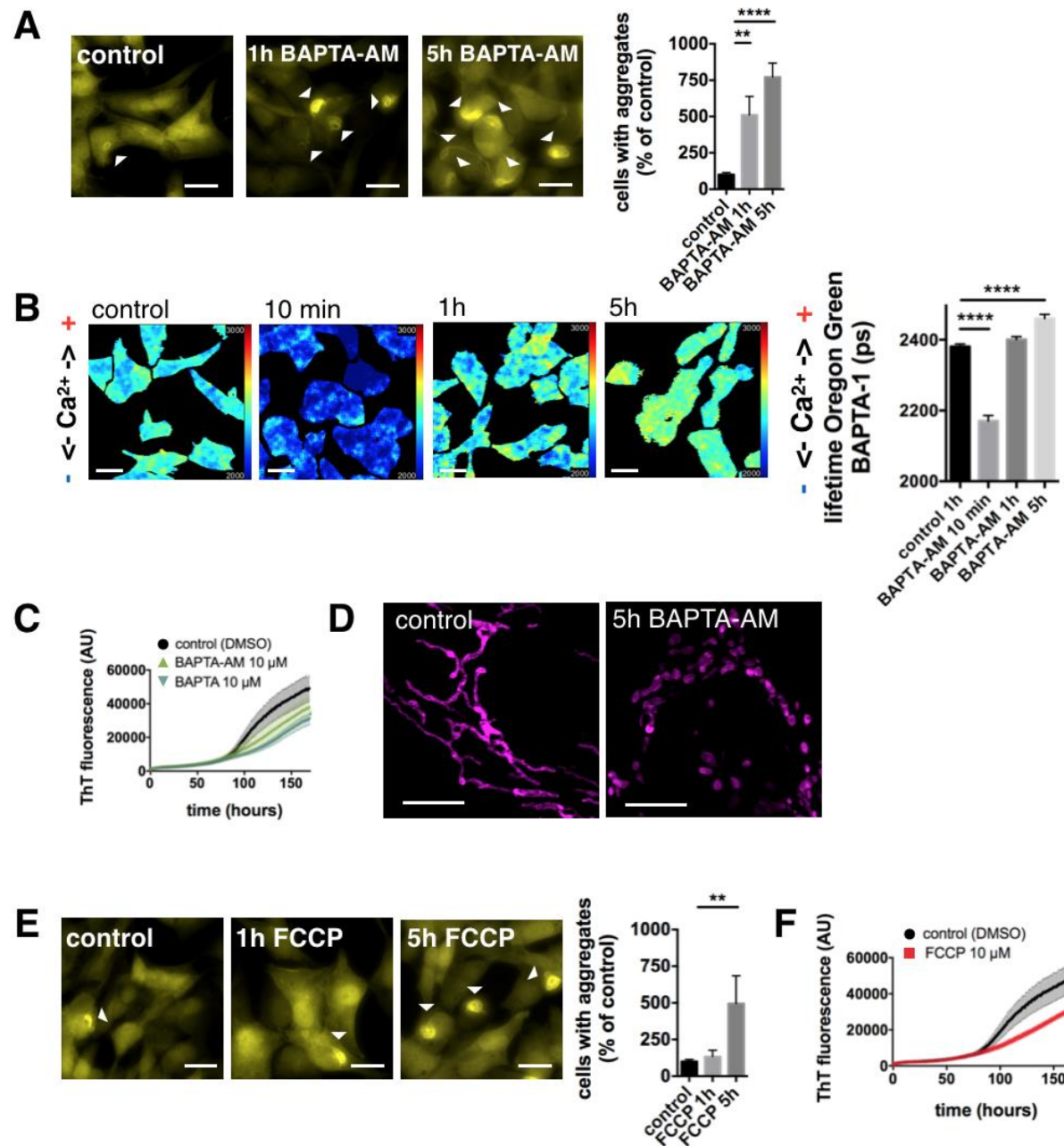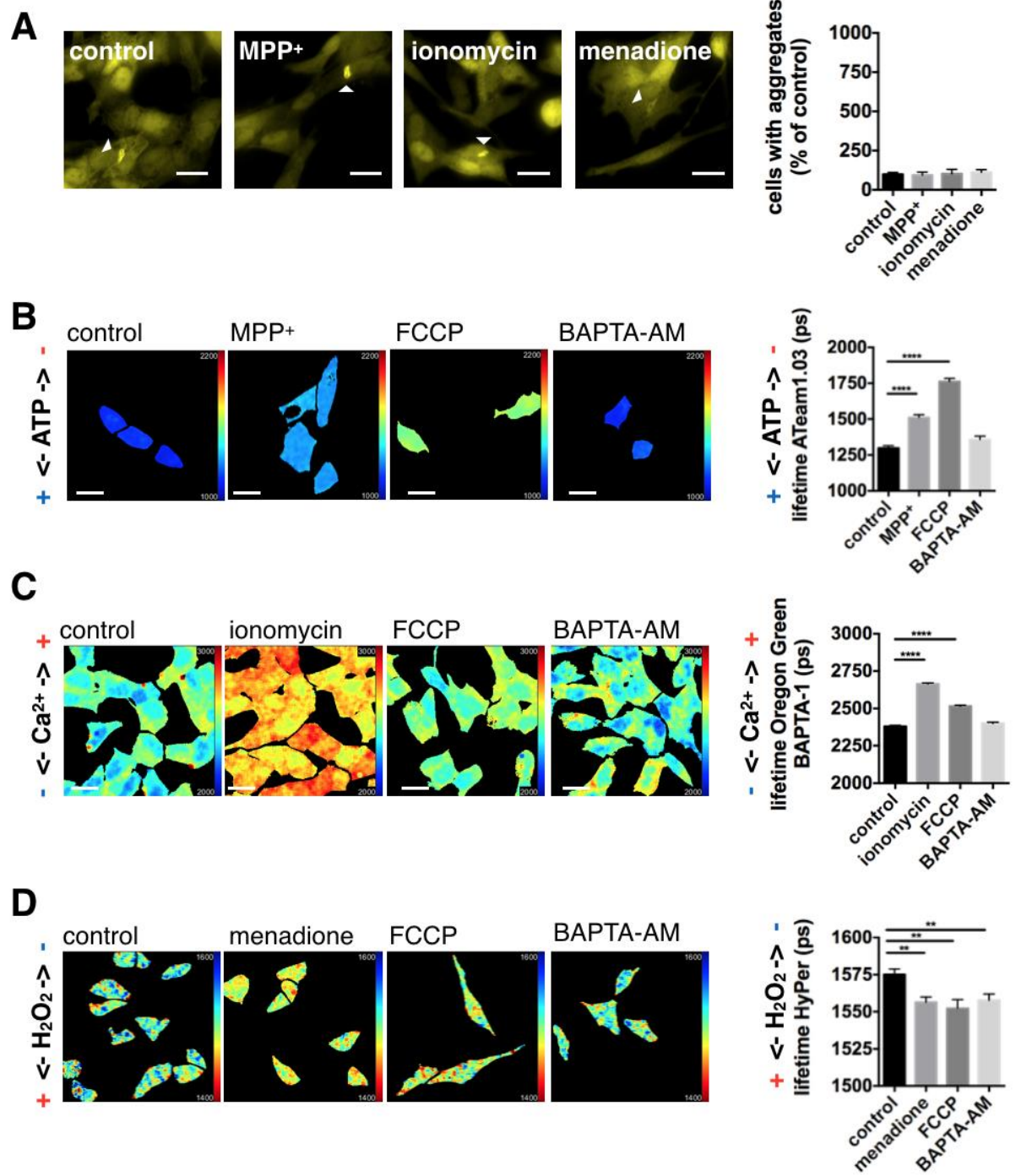1068

1069

1070

1071

1072

1073

1074

1075

1076

1077   **Figures**

1078   **Figure 1**

1079

1080

1081

1082

1083

1084

Figure 2

1091   **Figure 3**

1092

1093

1094

1095

1096

1097

1098

1099

1100

1101

1102

1103

1104   **Figure 4**

1105

1106

1107

1108

1109

1110

1111

1112

1113

1114

1115

50

1116   **Figure 5**

1117

1118

1119

1120

1121

1122

1123

1124

1125

1126

1127

1128

1129

1130

1131

51
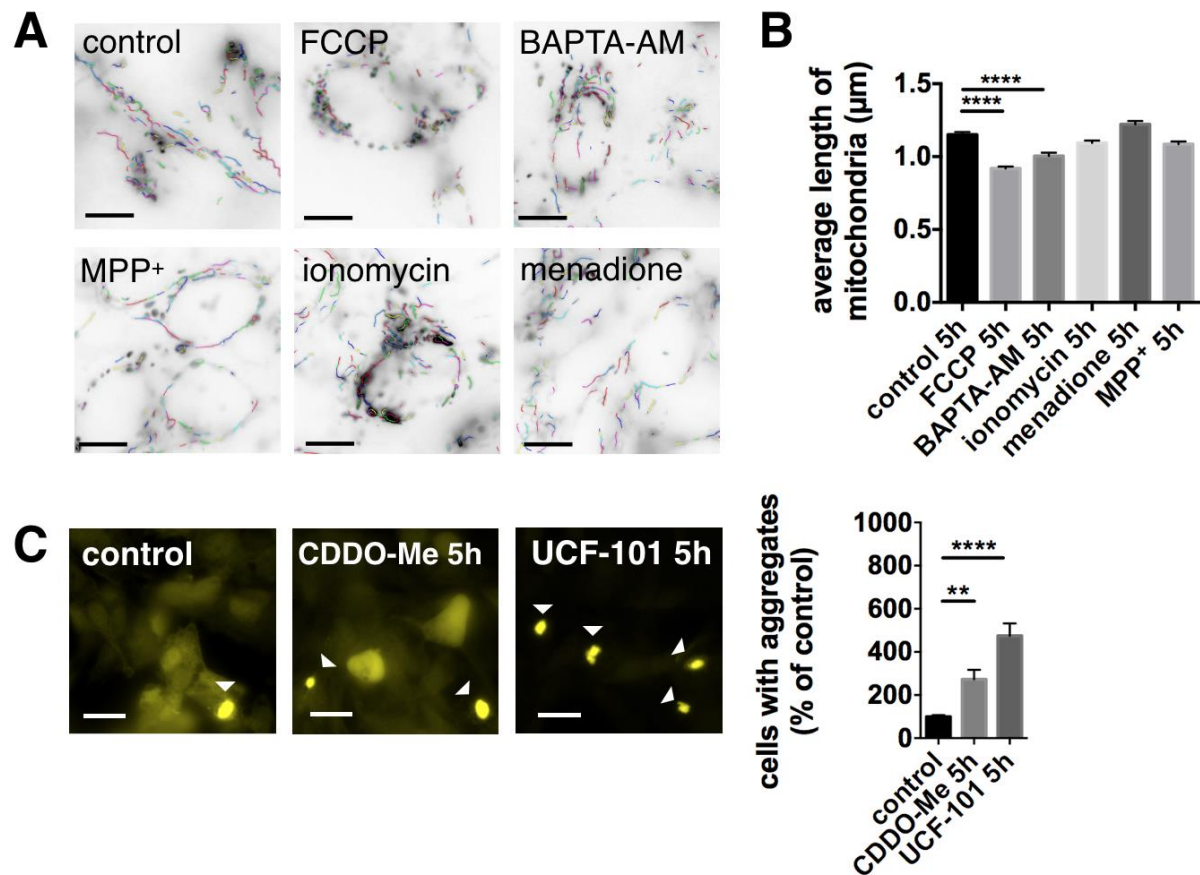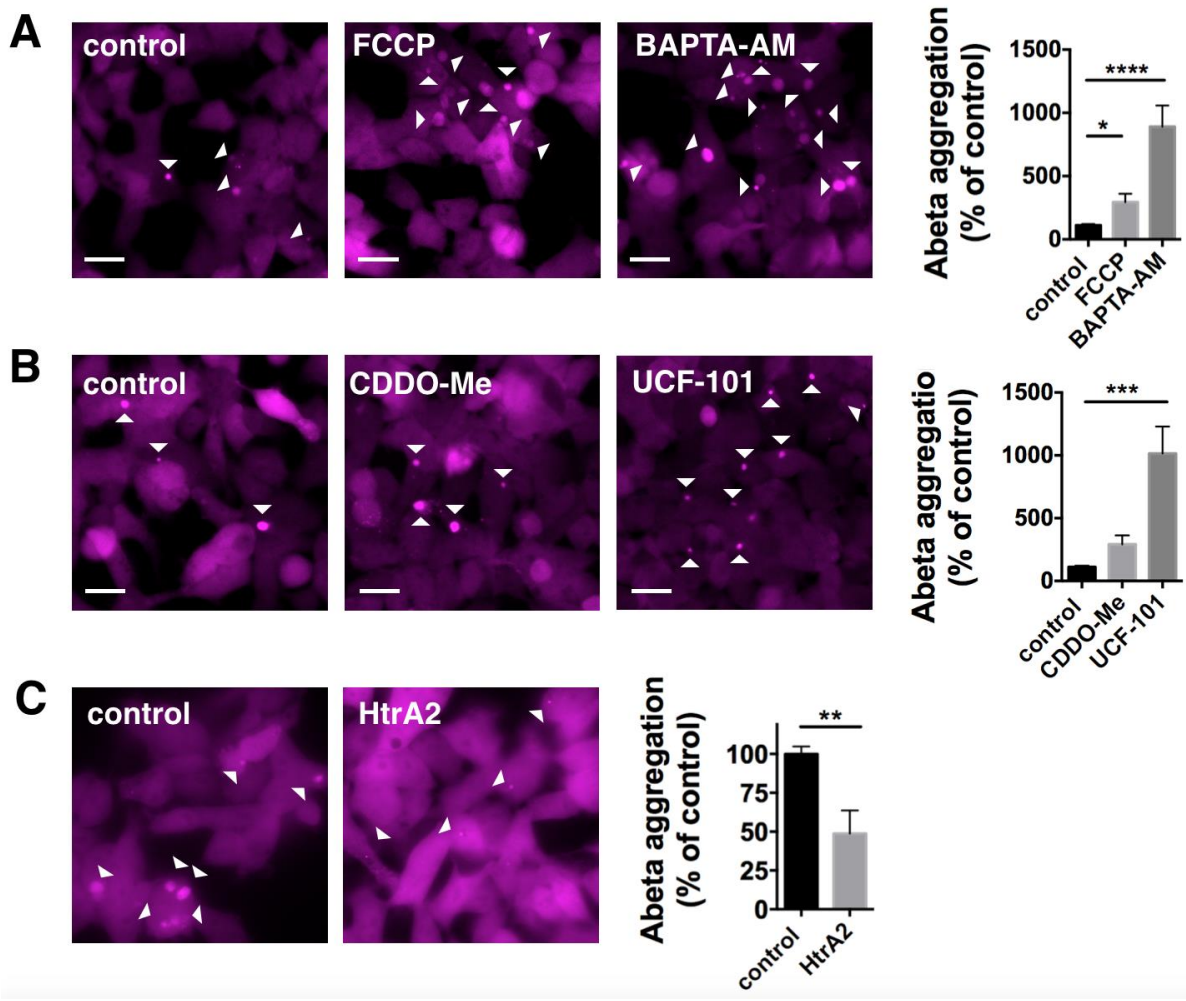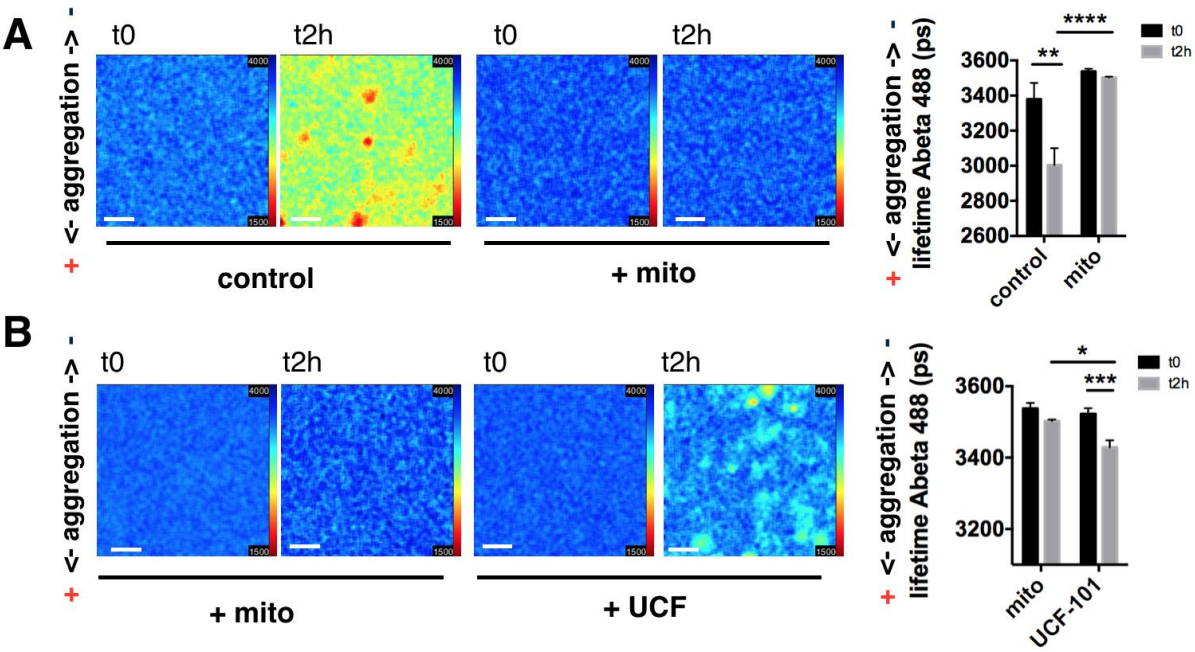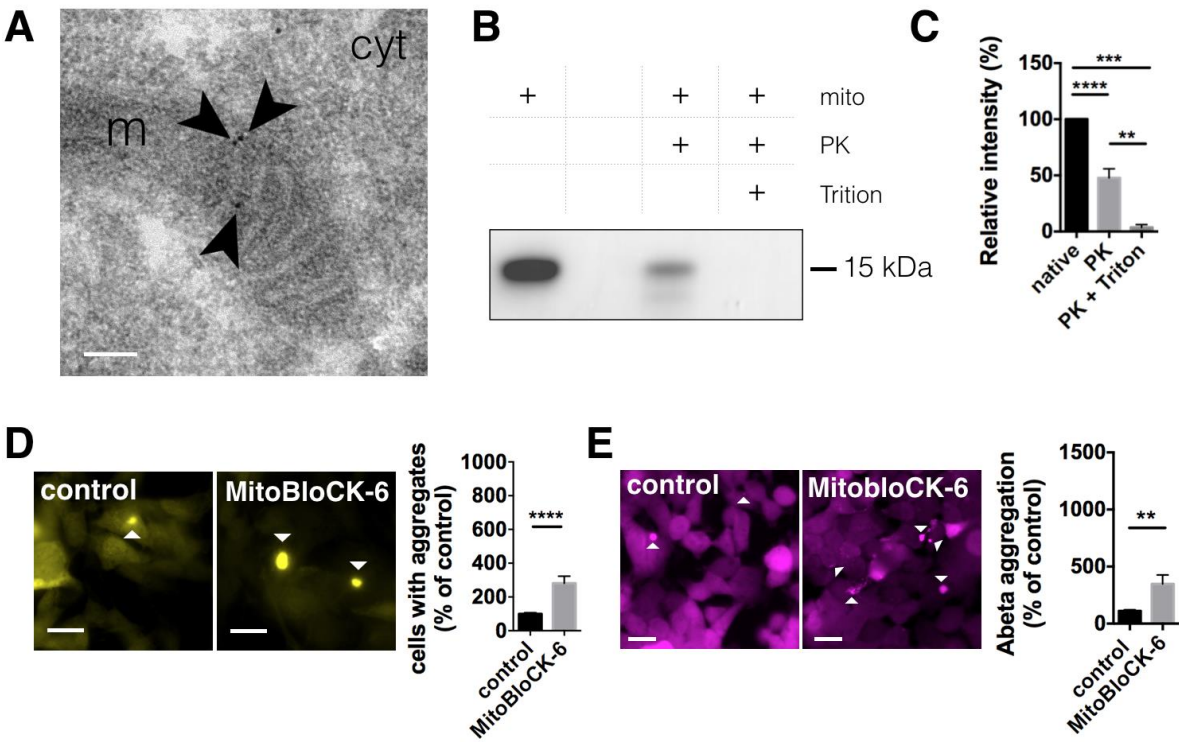
Figure 6

1147 **Supplementary Figure 1**

1148

1149

1150

1151

1152
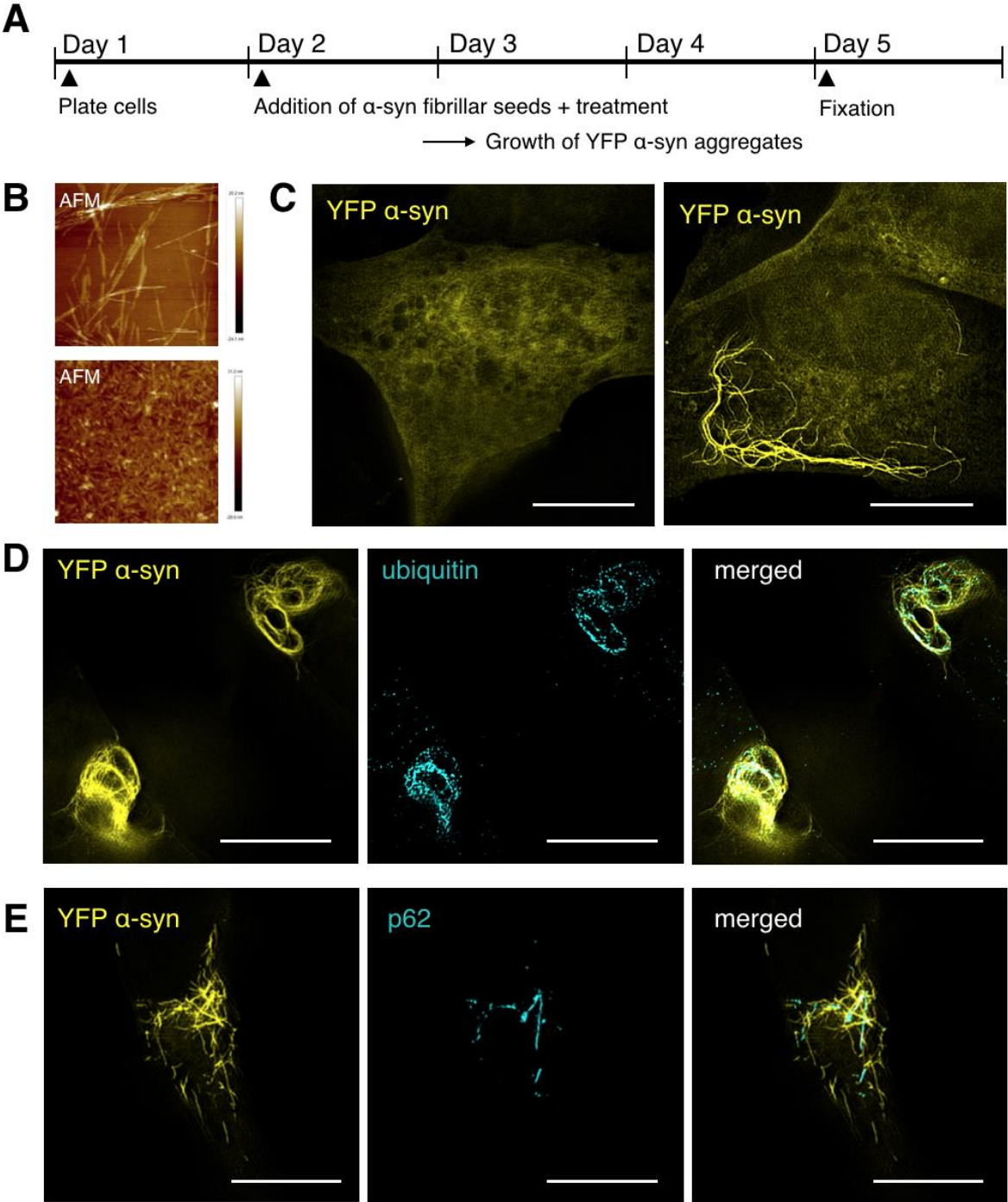
1153 **Supplementary Figure 2**

1154